Sulphur abundance in Galactic stars

Elisabetta Caffau, Piercarlo Bonifacio, R. Faraggiana, Patrick François, R. G. Gratton, Mauro Barbieri

A&A 441, 533–548 (2005)
DOI: 10.1051/0004-6361:20052905

Astronomy & Astrophysics

Sulphur abundance in Galactic stars⋆,⋆⋆

E. Caffau[1], P. Bonifacio[2], R. Faraggiana[3], P. François[4], R. G. Gratton[5], and M. Barbieri[5]

[1] Liceo L. e S.P.P. S. Pietro al Natisone, annesso al Convitto Nazionale "Paolo Diacono", Piazzale Chiarottini 8, Cividale del Friuli (Udine), Italy
e-mail: elcaffau@yahoo.it
[2] Istituto Nazionale di Astrofisica – Osservatorio Astronomico di Trieste, via Tiepolo 11, 34131 Trieste, Italy
e-mail: bonifaci@ts.astro.it
[3] Dipartimento di Astronomia, Università degli Studi di Trieste Trieste, via Tiepolo 11, 34131 Trieste, Italy
e-mail: faraggiana@ts.astro.it
[4] Observatoire de Paris, 64 Avenue de l'Observatoire, 75014 Paris, France
[5] Istituto Nazionale di Astrofisica – Osservatorio Astronomico di Padova, Vicolo dell'Osservatorio 5, 35122 Padova, Italy

Received 18 February 2005 / Accepted 20 May 2005

Abstract. We investigate sulphur abundance in 74 Galactic stars by using high resolution spectra obtained at ESO VLT and NTT telescopes. For the first time the abundances are derived, where possible, from three optical multiplets: Mult. 1, 6, and 8. By combining our own measurements with data in the literature we assemble a sample of 253 stars in the metallicity range $-3.2 \lesssim$ [Fe/H] $\lesssim +0.5$. Two important features, which could hardly be detected in smaller samples, are obvious from this large sample: 1) a sizeable scatter in [S/Fe] ratios around [Fe/H] ~ -1; 2) at low metallicities we observe stars with [S/Fe] ~ 0.4, as well as stars with higher [S/Fe] ratios. The latter do not seem to be kinematically different from the former ones. Whether the latter finding stems from a distinct population of metal-poor stars or simply from an increased scatter in sulphur abundances remains an open question.

Key words. stars: abundances – stars: population II – stars: kinematics – stars: atmospheres – Galaxy: halo – Galaxy: evolution

1. Introduction

Sulphur has been a long-neglected element in the study of Galactic chemical evolution; after the pioneering works of Clegg et al. (1981) for stars with [Fe/H] ≥ -1 and François (1987, 1988) for the most metal-poor stars, nothing was published until recent years. This light interest was largely due to the difficulty of measuring S abundances in stars, as detailed in the next sections, but also to the fact that since abundances of nearby α-elements Si and Ca were readily available from the analysis of stellar spectra, it was felt that the additional insight into nucleosynthesis and chemical evolution which could be derived from sulphur abundances was not worth the great effort necessary to measure them. From the nucleosynthetic point of view, sulphur is made by oxygen burning, like Si and Ca, either in a central burning phase, convective shell, or explosive phase according to Limongi & Chieffi (2003). This is a strong reason why Si, S, and Ca are expected to vary in lockstep with chemical evolution.

However, in recent years the study of chemical evolution in external galaxies has gained impetus. For this purpose, the more readily available objects are Blue Compact galaxies (BCGs, Garnett 1989; Torres-Peimbert et al. 1989) through analysis of the emission line spectra, and Damped Ly-α systems (DLAs, Centurión et al. 2000) through the analysis of resonance absorption lines. In both groups of objects sulphur, is relatively easy to measure. And for both groups of objects a gaseous component of the galaxy is measured, being always aware of possible corrections to the measured abundances for the fraction of elements which are locked in dust grains (depletions). From this point of view sulphur is a very convenient element to use because it is known from the study of the Galactic interstellar medium that sulphur is a volatile element, i.e. it forms no dust. It has thus become very interesting to provide a solid Galactic reference for sulphur abundances, which may be directly compared to measures in external galaxies.

Thus in recent years there have been a number of studies with this goal (Israelian & Rebolo 2001; Chen et al. 2002; Takada-Hidai et al. 2002; Chen et al. 2003; Nissen et al. 2004; Ryde & Lambert 2004; Ecuvillon et al. 2004), leading to a somewhat controversial picture. Some studies claim that sulphur behaves exactly like silicon and other α elements (Chen et al. 2002, 2003; Nissen et al. 2004; Ryde & Lambert 2004),

⋆ Based on observations collected at ESO in programmes: 056.E-0665, 59.E-0350, 62.L-0654 and 165.L-0263.
⋆⋆ Appendix A is only available in electronic form at http://www.edpsciences.org

which display a "plateau" in their ratios to iron, while other studies seem to favour a linear increase of [S/Fe] ratios with decreasing metallicities (Israelian & Rebolo 2001; Takada-Hidai et al. 2002).

To shed new light on the problem of the evolution of sulphur in the Galaxy, we analyse high resolution spectra of Galactic stars that were collected in the course of several of our observational programmes, as well as spectra retrieved from the ESO archive.

2. Observational data

The sample of stars was obtained by combining observations made at ESO with the NTT and VLT telescopes (see Table A.1). In this table we report the *S/N* ratio at 670 nm, when available, otherwise we report the *S/N* ratio at 870 nm. The spectra of most stars were already used for different investigations and the observational details published in other papers.

2.1. NTT spectra

NTT data were obtained in three different runs, programmes 56.E-0665, 59.E-0350, and 62.L-0654. The data of programme 56.E-0665 were retrieved from the ESO archive. The observations were obtained in January 1996, and abundances from several elements derived from these spectra were presented by Nissen & Schuster (1997). The EMMI instrument configuration used was echelle # 14 and grism # 3 as a cross-disperser, and the resulting resolution was $R \sim 60\,000$. These spectra are marked as ESONTTB in the last column of Table A.1. We performed the observations of programmes 59.E-0350 and 62.L-0654 in August 1997 and March 1999, respectively. In both cases the EMMI instrument was used with echelle # 14 and grism # 6 as cross-disperser; also in this case the resolution was $R \sim 60\,000$. These spectra are marked as ESO-NTT in the last column of Table A.1. The different cross-dispersers and central wavelengths result in different spectral coverage, nevertheless for all NTT data the only S I lines available were those of Mult. 8.

2.2. VLT spectra

All VLT data were obtained in the course of the Large Programme 165.L-0263 (P. I. R. G. Gratton), which used the UVES spectrograph mounted on the Kueyen-VLT 8.2 m telescope at Paranal. For most observations the slit width was 1″ yielding a resolution $R \sim 43\,000$, and occasionally, due to variable seeing conditions, slightly smaller or larger slit widths were used. The data for all the stars in the present paper were also used by Gratton et al. (2003). All observations were taken with dichroic # 2 and grating # 4 as cross disperser. Only the red arm spectra are discussed here; in the first run of June 2000, the central wavelength of the red arm was set to 700 nm, which allows one to cover the range 520−890 nm with a small gap between 700 nm and 705 nm, corresponding to the gap in the red arm CCD mosaic. Therefore for this run, only the S I lines of Mult. 6 and 8 are available. In all subsequent runs the central wavelength was set at 750 nm, thus allowing coverage of the range 575−931 nm, with a gap of about 5 nm around 750 nm. Therefore for this set of data all three S I multiplets discussed in this paper, i.e. Mult. 1, Mult. 6, and Mult. 8, are available.

3. Atmospheric parameters

Most stars studied here are in common with Gratton et al. (2003); we adopted their values of the atmospheric parameters $T_{\rm eff}$, $\log g$, and [Fe/H], in order to compare [S/Fe] to their value of [Mg/Fe]. For the other stars, we used IRFM temperatures from Alonso (private communication) and surface gravities derived from the Hipparcos parallax (Eq. (5) of Gratton et al. 2003), whenever available, or from the Fe I/Fe II ionization balance, otherwise. For the remaining stars we used the atmospheric parameters of Nissen & Schuster (1997). The errors on $T_{\rm eff}$ are about 50 K according to Gratton et al. (2003) and about 40 K according to Nissen & Schuster (1997). The error on IRFM temperatures is larger, on the order of 100 K. The internal error on $\log g$ from Hipparcos-based parallaxes is on the order of 0.1 dex and is dominated by the error on the parallax. The error on surface gravities based on Fe I/Fe II ionization balance is again on the order of 0.1 dex (Nissen & Schuster 1997).

The choice of the microturbulence (ξ) does not affect the S-abundance determination from the weak lines of Mult. 6 and 8, but may be important for the stronger lines of Mult. 1 for the less metal poor stars (see Sect. 6). To analyse the lines of all multiplets, we adopted the ξ value in Gratton et al. (2003). For multiplets 6 and 8 we adopted the $\xi = 1$ km s^{-1} when Gratton et al. (2003) was not available.

4. The S I spectrum

Preliminary work consisted in selecting lines which can be measured on spectra of metal-poor stars and retrieving the most reliable log gf values.

4.1. Choice of S I lines

In the S I spectrum the lowest levels transitions belonging to the triplet system lie in the UV below 200 nm and the "raie ultime" is at 180.731 nm; however, in this region the flux of F-G stars is too low to be easily observable. The S abundance in these stars can be derived from the strongest lines in the optical range, which belong to the quintet system with the lowest energy level at 52623.640 cm^{-1}.

A preliminary selection of S I lines at wavelengths shorter than 950 nm was made on the basis of their intensity in the Revised Multiplet Tables (RMT) (Moore 1972), the Utrecht Solar Atlas (Moore et al. 1966), Lambert & Warner (1968, LW, hereafter), and Biemont et al. (1993, BQZ, hereafter). The synthetic spectrum of the Sun was computed and compared with the solar spectrum of the solar atlas of Kurucz et al. (1984) and used as a guideline.

The strongest lines in the visual-near IR spectrum are those of Mult. 1, 2, 6, and 8. The lines of Mult. 2 were discarded; the strongest line, 469.4113 nm, is weak and blended with Cr I 469.4099 nm in the Sun. Some of the lines of Mult. 6 were

also discarded on the basis of their appearance in the solar spectrum. Line 868.046 nm is blended with a Si I line with uncertain log *gf*, and its intensity in the solar spectrum does not agree with what is predicted by the computed spectrum. The lines at 867.065 nm (RMT = 867.019 nm (J = 1−0), 867.065 nm (J = 1−1), 867.137 nm (J = 1−2)) were discarded, because they are too weak to be measured in the spectra of metal-poor stars. The lines of Mult. 7 were not considered, since their low intensity in the solar spectrum makes them useless for sulphur measurements in metal-poor stars. We point out that the intensities given in RMT for these lines are not coherent with the line strengths observed in the Sun.

Other rather strong lines, but with higher excitation potentials, are those of:

- Mult. 10: the 604.1 nm line is weak in the solar spectrum (LW) and blended with Fe I according to the Utrecht Solar Atlas. We note that the Fe I line is weak in our computed spectrum. Identification of the 604.5 nm line as S I is doubtful according to LW; according to the Utrecht Solar Atlas it is affected by telluric lines. However, at this wavelength no telluric lines are detected in our spectra of fast rotators. The line at 605.2 nm is not blended in the Sun and our computed spectrum provides an excellent fit; however, its low intensity would make it measurable only in moderately metal-poor stars. The latter two lines were used by Chen et al. (2002), who discarded the 604.5 nm anyway in their solar analysis, because they noted the presence of an unidentified blend in the blue edge of the line. They claim, however, that the two lines provide consistent S abundances in their stars, which suggests that the blending feature disappears at metallicities just below solar.
- Mult. 13: all the lines are weak in the solar spectrum (LW); the strongest line, 903.588 nm, is blended with a Cr II line. A further reason for discarding this multiplet is that LW noted that they give a smaller S abundance in the Sun.
- Mult. 21: all lines are easily measurable in the Sun, but are too weak to be measured at the resolution of our spectra.
- Mult. 22: all lines are blended with stronger lines in the solar spectrum, and their *gf* values are uncertain.

The selected lines for our S abundance measurements are those of Mult. 1, 6, and 8 listed in Tables 1−3 respectively. Concerning the lines of Mult. 8, we note the inconsistency of the *EW*s in the Utrecht Solar Atlas (0.5 and 1.2 pm) with those of LW (1.7 and 1.2 pm) and also with the relative intensities of the 674.8 nm and 674.3 nm lines in the RMT (8 and 6).

4.2. Atomic data

The lines of Mult. 1 were measured in stellar spectra only by Nissen et al. (2004) and Ryde & Lambert (2004). They are strong but difficult to measure due to the blending and to the presence of telluric lines. Line 921.2863 nm is blended with the weak Fe I line 921.2970 nm; line 922.8093 nm is near the core of Paschen ζ (922.9017 nm), and line 923.7538 nm is on the far wing of the same Paschen line and near the Si I 923.8037 nm line.

Table 1. Transitions and log *gf* of Mult. 1: LW = Lambert & Warner (1968); Wiese = Wiese et al. (1969); BQZ = Biemont et al. (1993) and RL = Ryde & Lambert (2004).

	Transition	λ (nm)	LW	Wiese	BQZ	RL
4s–4p	$^5S^\circ_2$–$^5P_1$	923.7538	–0.01 (*)	0.04	0.10	0.04
	$^5S^\circ_2$–$^5P_2$	922.8093	0.23	0.26	0.32	0.25
	$^5S^\circ_2$–$^5P_3$	921.2863	0.38	0.42	0.47	0.43

(*) This is the value given by Lambert & Warner (1968); Lambert & Luck (1978). Nissen et al. (2004) use the value +0.01.

Table 2. Transitions and log *gf* of Mult. 6: LW = Lambert & Warner (1968); W = Wiese et al. (1969); Fr = François (1987); BQZ = Biemont et al. (1993); C = Chen et al. (2002, 2003).

	Transition	λ (nm)	LW	W	Fr	BQZ	C
4p–4d	$^5P_3$–$^5D^\circ_3$	869.3931	–0.56	–0.51	–0.74	–0.85	–0.52
	$^5P_3$–$^5D^\circ_4$	869.4626	0.03	0.08	–0.21	–0.26	0.05

Table 3. Transitions and log *gf* of Mult. 8: LW = Lambert & Warner (1968); Wiese = Wiese et al. (1969); BQZ = Biemont et al. (1993) and Ecu = Ecuvillon et al. (2004).

	Transition	λ (nm)	LW	Wiese	BQZ	Ecu
4p–5d	$^5P_1$–$^5D^\circ_0$	674.3440	–0.85	–1.27	–1.20	–1.27
	$^5P_1$–$^5D^\circ_1$	674.3531	–	–0.92	–0.85	–0.92
	$^5P_1$–$^5D^\circ_2$	674.3640	–1.12	–1.03	–0.95	–0.93
	$^5P_2$–$^5D^\circ_1$	674.8573	–1.48	–1.39	–1.32	–
	$^5P_2$–$^5D^\circ_2$	674.8682	–0.48	–0.80	–0.73	–
	$^5P_2$–$^5D^\circ_3$	674.8837	–	–0.60	–0.53	–
	$^5P_3$–$^5D^\circ_2$	675.6851	–0.94	–1.76	–1.67	–
	$^5P_3$–$^5D^\circ_3$	675.7007	–	–0.90	–0.83	–0.81
	$^5P_3$–$^5D^\circ_4$	675.7171	–0.40	–0.31	–0.24	–0.33

Chen et al. (2003) ignore the fine structure of the line and adopt log *gf* = –0.70 for 674.36 nm and log *gf* = –0.31 for 675.717 nm.

The lines of Mult. 1 are almost ten times stronger than those of Mult. 6 so that they allow measurement of S abundance for very metal poor stars. The oscillator strengths of the lines of this multiplet measured by Wiese et al. (1969) agree with those computed by LW and also with those computed by BQZ, as can be seen from Table 1. Ryde & Lambert (2004) use the NIST database (Sansonetti & Martin 2004). Nissen et al. (2004) use Lambert & Luck (1978), which are the same as LW, except for the 923.7538 nm line. We adopt the log *gf* values of the NIST database, which holds the values of Wiese et al. (1969), which are experimental but of D quality, corresponding to a possible error up to 50%. The same choice has been adopted for the other multiplets.

In literature most S abundances are derived from the two strongest lines of Mult. 6. These are the only lines used by

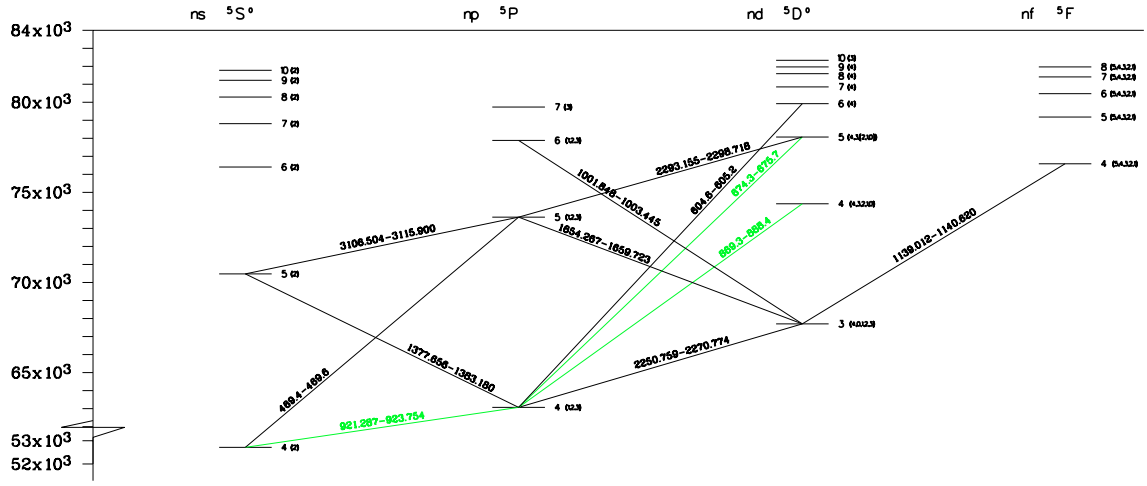

Fig. 1. Grotrian diagram of the Quintet system. The decays that give rise to the lines of multiplets 1, 6, 8 are indicated in grey. The partial Grotrian diagram of the quintet system, including the lines of astrophysical interest, was adapted from Atomic energy-level and Grotrian diagrams by Bashkin & Stoner (1978).

Clegg et al. (1981), by François (1987, 1988) and by Israelian & Rebolo (2001).

Part of the differences in the sulphur abundances found in the literature using the lines of Mult. 6 may be tracked back to the log *gf* values adopted by the different authors; in fact these lines display the largest discrepancies among available log *gf* values.

Clegg et al. (1981) used the values of Lambert & Warner (1968), which are also used by Lambert & Luck (1978) for the solar spectrum and by Nissen et al. (2004). François (1987) derived "solar" oscillator strengths from the Moon spectrum obtained with the same spectrograph he used for the stellar spectra. Israelian & Rebolo (2001) used Wiese et al. (1969)[1]. Biemont et al. (1993) computed theoretical oscillator strengths using both a Hartree-Fock relativistic code (HFR) and the formalism implemented in the SUPERSTRUCTURE (SST) code, and obtained a good agreement between the two approaches. They recommend HFR values because they are available for a larger set of lines. According to these authors, their log *gf* should in general be more accurate than those of both LW and Wiese et al. (1969). It is significant, however, that the two lines 869.40 nm and 869.47 nm are not retained in the BQZ determination of the solar S abundance. For this reason we decided not to adopt the oscillator strengths of BQZ.

The lines of Mult. 8 are free of blends and arise from the same lower level as those of Mult. 6, so that the dependence of these two sets of lines on $T_{\rm eff}$ and log g of the stars is the same. The oscillator strengths used by different authors are in agreement: LW, Wiese et al. (1969) and BQZ, and also Ecuvillon et al. (2004) who adopted VALD data modifying them to obtain a good fit to the solar spectrum. For Mult. 8 the log *gf* measured by Wiese et al. (1969) and those computed by BQZ and LW are similar.

[1] They used the values of VALD database which for S I contains the data in Kurucz (1993), which, in turn, contains the Wiese et al. (1969) measurements.

Table 4. Spectrum with T = 5800 K, log g = 4.25, [Fe/H] = −1.5, [S/H] = −1.10 for the lines of Mult. 8. Each Monte Carlo simulation includes 500 events.

S/N	*A*(S)	Error
300	6.11	0.05
250	6.10	0.06
200	6.10	0.07
150	6.10	0.08
100	6.10	0.13
80	6.10	0.17
50	6.14	0.21
30	6.18	0.29

The problem of the high discrepancies among log *gf* values appears to be restricted to the two lines of Mult. 6. Our tests show that the BQZ log *gf* of Mult. 6 lines produces S abundances not coherent with those derived from Mult. 8, strengthening our choice of not adopting this source.

From Tables 1–3 we conclude that literature data need not be scaled, because the adopted log *gf* values are compatible. The differences in adopted log *gf* values are within the random errors of S abundance determinations.

4.3. S abundance in the Sun

We note small differences in the solar S abundance used by the quoted authors. The value $A(\mathrm{S})_\odot$ = 7.21 (Anders & Grevesse 1984, 1989) is used by François (1987, 1988) and Israelian & Rebolo (2001). Chen determined $A(\mathrm{S})_\odot$ = 7.20, a value adopted by Nissen et al. (2004) and Ryde & Lambert (2004); Takada-Hidai et al. (2002) use $A(\mathrm{S})_\odot$ = 7.21 for their HIRES sample, and 7.22 for their OAO sample because this is the sulphur solar abundance they derived. The only discrepant value is BQZ A(S) = 7.33 adopted by Grevesse et al. (1996) and Grevesse & Sauval (1998).

Chen et al. (2002) in the Notes of Table 4 say that "the α enhancement for S is calculated assuming $A(\mathrm{S}) = 7.33$ for the Sun following Grevesse & Sauval (1998)". In his models Kurucz retains $A(\mathrm{S}) = 7.21$, i.e. the value of Lambert & Warner (1968) and Anders & Grevesse (1989); the same selection is made by Lodders (2003) for the solar photospheric value. We finally recall $A(\mathrm{S}) = 7.14$ by Asplund (2004) who used a 3D hydrodynamical model. We did not consider this value because it is not directly comparable to our results obtained from 1D models.

4.4. Predicted intensity of S I lines in stellar spectra

In the metallicity range of our sample, the use either of α-enhanced or non α-enhanced models affects the derived sulphur abundances by a few hundredths of dex at most, as already shown by Chen et al. (2002).

Sulphur abundance is dependent on $T_{\rm eff}$ and $\log g$, as well as on the metallicity of the star. In fact $A(\mathrm{S})$ increases with increasing $T_{\rm eff}$, while it decreases, at constant $T_{\rm eff}$ value, with decreasing gravity.

5. Analysis

5.1. Model atmospheres and synthetic spectra

For each star we computed a model atmosphere using version 9 of the ATLAS code (Kurucz 1993) running under Linux (Sbordone et al. 2004). We used the updated Opacity Distribution Functions of Castelli & Kurucz (2003) with microturbulent velocity of 1 km s^{-1} and enhancement of α elements. The synthetic spectra were computed using the SYNTHE suite (Kurucz 1993) running under Linux (Sbordone et al. 2004).

5.2. Line profile fitting

In the present investigation we decided to determine abundances by making use of line profile fitting. This approach is required for the lines of Mult. 1 which, as discussed above, are affected by the wings of Paschen ζ; and it is also desirable for the lines of Mult. 8, which are affected by fine structure splitting, although one could ignore the fine structure since the lines are weak. In principle, the lines of Mult. 6 which were used are isolated and could be treated efficiently by simply measuring the equivalent width. However, we decided to also use line profile fitting in this case for two reasons: first for homogeneity with what was done for the other lines, and second because these lines are often weak, especially at the lower metallicities. The inclusion of fitting continuum and neighbouring lines with a synthetic spectrum greatly improved the stability of the fitting procedure with respect to fitting a single Gaussian to measure the equivalent width.

We developed a line fitting code which performs a χ^2 fit to the observed spectrum. The best fitting spectrum is obtained by linear interpolation between three synthetic spectra which differ only in their S abundance; the minimum χ^2 is sought numerically by making use of the `MINUIT` routine (James 1998). As pointed out by Bonifacio & Caffau (2003) the χ^2 theorems do not apply to the fitting of spectra, because the pixels are correlated[2]. However, χ^2 minimization may still be used to estimate parameters (in our case abundances), but errors cannot be deduced from χ^2 (Press et al. 1992). In fact, as described in the next section, we resort to Monte Carlo simulations to estimate errors.

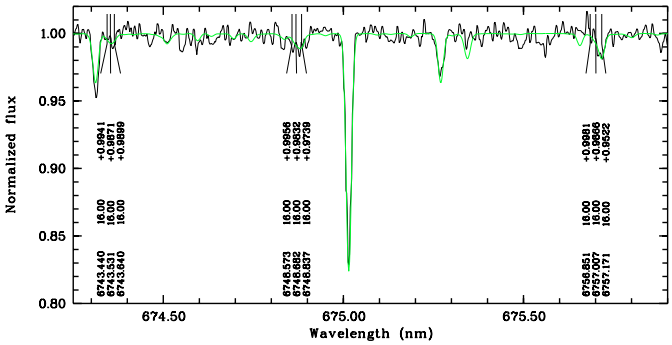

Fig. 2. Fit in the region of 670 nm of the star HD 25704 (black observed spectrum, grey fitted spectrum). The Fe I 675.0152 is in good agreement with the [Fe/H] utilized, so we fitted the whole range including the S I lines of Mult. 8 and the lines of other elements as well.

The fitting code works interactively under `MIDAS`: the user selects the spectral region to be fitted by using the graphic cursor. For sulphur we selected regions containing one or more S I lines and in some cases also lines of other elements. In the region of Mult. 8, all the 3 S I lines[3] were fitted simultaneously. This region also includes the Fe I 675.0152 nm line and some weak lines of other elements. An example is given in Fig. 2. The presence of the Fe I line does not disturb the fit; on the contrary, it helps make it more stable, especially in cases in which the adopted Fe abundance fits the observed line well. In those cases in which the adopted Fe abundance is not in agreement with the line strength of this particular line, or when only one of the S I lines is detectable or the spectrum is affected by bad pixels, cosmic ray hits, etc., the fit was made on a single S I line. The same criterion was used for the Fe I 868.8624 nm: for the lines of Mult. 6 an example is shown in Fig. 3.

In the region of Mult. 1, each S I line was fitted individually because of the telluric lines affecting the spectrum. In a first step the regions affected by telluric lines were identified by using the spectrum of a fast rotator, and if a telluric line was blending an S I line, this was not used. An example of a fit of a Mult. 1 line is shown in Fig. 4.

In a second step we tried to use the spectrum of a fast rotator, suitably scaled, to remove the telluric absorptions which are affecting S I lines. The spectra of fast rotators at our disposal were not ideal since they were seldom observed on the same night as our programme stars and hardly ever at the same airmass. Under these conditions the removal of the tellurics is

[2] In fact, on the one hand, in most spectrographs the slit projects on at least two pixels, thus making the signal in neighbouring pixels correlated; on the other hand, one usually works on spectra which were rebinned to a constant wavelength step, in order to allow the coaddition of different spectra, often with an oversampling factor of at least 2. Therefore neighbouring pixels are strongly correlated.

[3] At our resolution, the fine structure is not resolved, although the "lines" are really a blend of three lines.

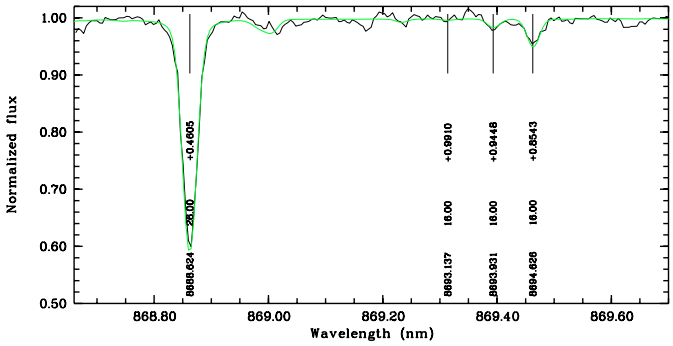

Fig. 3. Fit in the region of Mult. 8 of the star HD 10607; black is the observed spectrum and grey the fit.

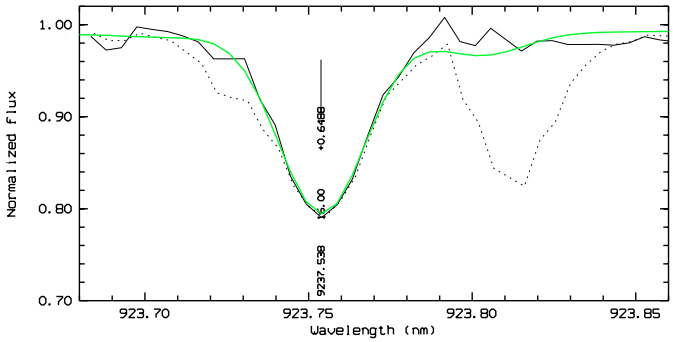

Fig. 4. Fit in the region of Mult. 6 of the star HD 10607. The solid line is the observed spectrum after subtraction of telluric lines; dotted line is observed spectrum, grey is the fit.

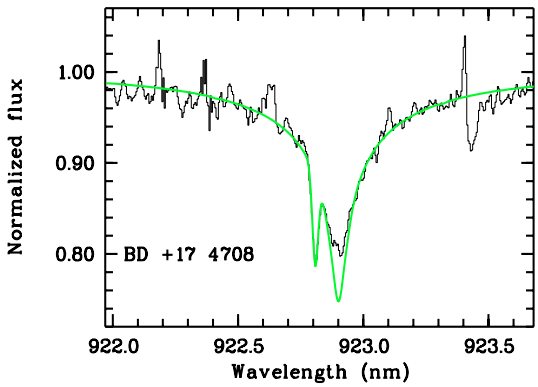

Fig. 5. Fit of the 922.8 nm S I line in star BD +17 408. It may be appreciated that the synthetic spectrum provides a good fit to the wings of Paschen ζ, while not to the core. This is not surprising since our synthetic spectra are computed in LTE and the core of Paschen lines is predicted to be affected by NLTE effects (see for example Johnson & Kinglesmith 1965).

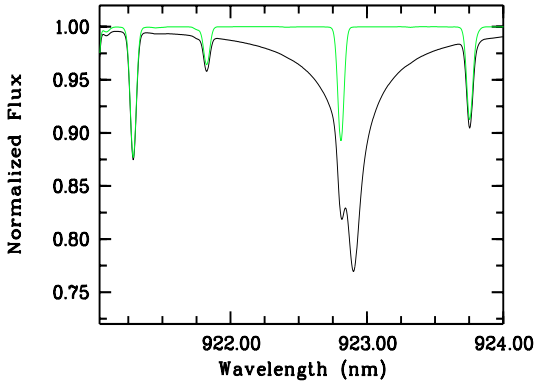

Fig. 6. Two spectra with parameters: $T_{\rm eff}$ = 6016 K, $\log g = 4.04$, and [Fe/H] = –1.5, the G 126 –62 star parameters. The black one is the one we used to fit the sulphur abundance, while the grey one is built without the 922.9017 nm Paschen ζ.

rather unstable. In fact, it can happen that their removal produces a clean S I line, but in some cases this line implied an abundance in dire disagreement with that measured from lines unaffected by the tellurics, and thus the procedure was unsuccessful. We conclude that, under these conditions, we would retain the measures on lines from which a contaminating telluric was removed only in those cases in which at least one of the three lines was unaffected by tellurics and the abundances derived from both contaminated and uncontaminated lines were in agreement.

In theory one should be able to deduce the sulphur abundance for lines of Mult. 1 from the equivalent widths (*EW*s). In practice, the three sulphur lines lie next to the Paschen ζ line. The 922.8093 nm line is next to the core of Paschen ζ and it is impossible to measure its true equivalent width. But the 921.2863 nm and 923.7538 nm S I lines are also affected by the wings of Paschen ζ and, moreover, the former is blended with a weak Fe I line (921.297 nm), and the latter is blended with Si I 923.8037 nm. These two blending lines are so weak that they could be ignored.

To illustrate the effect of Paschen ζ and support our statement that spectrum synthesis is needed to study sulphur in this region, we computed two synthetic spectra with $T_{\rm eff}$ = 6016 K, $\log g$ = 4.04, and [Fe/H] = −1.5 (parameters of star G 126−62), one with Paschen ζ and the other without it (see Fig. 6). It may be appreciated that the *EW* of the 921.2863 nm line is almost the same in both cases, while the *EW* of the 923.7538 nm is larger in the spectrum computed without the hydrogen line. Going from *EW*s to abundances, one finds that matching a measured *EW* to one computed ignoring Paschen ζ, an S abundance that is lower by 0.08 dex is derived.

In measuring the *EW*, one is forced to use the wing of Paschen ζ as a local continuum, effectively underestimating the true *EW*. We performed a few experiments by measuring this *EW* on the synthetic spectrum and found that this underestimated the S abundance by an additional 0.08 dex. This effect of Paschen ζ on the 921.2863 nm sulphur line is instead negligible, as already stated by Nissen et al. (2004).

With this discussion we hope we have convinced the reader that the use of spectrum synthesis is definitely preferable to the use of *EW*s to derive S abundances from lines of Mult. 1. Table 6 reports sulphur abundances derived (when measurable) from each multiplet, the weighted average and the relative error.

Table 5. Spectrum with T = 5800 K, $\log g = 4.25$, [Fe/H] = −1.5, [S/H] = −1.10. Each Monte Carlo simulation has 500 events.

T K	$\log g$ cgs	[Fe/H]	ξ	A(S)	$\sigma_{\rm ran}$	$\sigma_{\rm sys}$
5600	4.25	–1.5	1.00	6.28	0.10	+0.17
5700	4.25	–1.5	1.00	6.17	0.10	+0.06
5900	4.25	–1.5	1.00	6.05	0.11	–0.06
6000	4.25	–1.5	1.00	6.00	0.11	–0.11
5800	4.00	–1.5	1.00	6.03	0.10	–0.08
5800	4.50	–1.5	1.00	6.18	0.10	+0.07
5800	4.25	–1.0	1.00	6.34	0.10	+0.23
5800	4.25	–1.3	1.00	6.14	0.08	+0.03
5800	4.25	–1.4	1.00	6.12	0.09	+0.01
5800	4.25	–1.6	1.00	6.10	0.09	–0.02
5800	4.25	–1.7	1.00	6.08	0.10	–0.03
5800	4.25	–2.0	1.00	6.01	0.14	–0.10
5800	4.25	–1.5	1.50	6.18	0.14	+0.07

6. Errors and sensitivity of abundances to stellar parameters

For reasons stated in the previous section, one cannot rely on the χ^2 theorems to obtain error estimates; we, therefore, resorted to a Monte Carlo method. We first estimated the statistical error: a synthetic spectrum with parameters representative of our stars was computed and Poisson noise was injected to obtain the desired *S/N* ratio. We shall refer to this as a "simulated observation". This spectrum was fitted in a similar way to the observed spectrum and the fitted parameters were derived. The process was repeated 500 times for the lines of Mult. 8, which are the weakest of the three multiplets considered here. The results are given in Table 4, where the mean derived abundance and the dispersion around this mean value are reported for different *S/N* ratios. The dispersions may be taken as estimates of the statistical errors. It is interesting to point out that small offsets exist in the mean derived abundance: at low *S/N* ratios the S abundance is overestimated by hundredths of dex, while at very high *S/N* ratios the abundance is underestimated by 0.01 dex.

In the case of incorrect atmospheric parameters, we also tried to estimate systematic errors, or rather the combination of systematic and statistical errors. The same procedure as described above was applied. However, we tried to fit our simulated observations with synthetic spectra whose atmospheric parameters were different from those of the simulated observation. We explored the effect of one parameter at the time: temperature, gravity, and Fe abundance. The systematic errors are estimated as the difference between the sulphur abundance of the simulated spectra and the mean fitted sulphur abundance. The results for the lines of Mult. 8 are given in Table 5. We further checked the variation of the systematic error with $T_{\rm eff}$ when changing $T_{\rm eff}$ in the range 5000 to 6000 K by simply using the WIDTH code. An error of 100 K implies an error in the sulfur abundance of ∼0.05 dex around 6000 K and ∼0.09 dex around 5000 K. These results, together with those of Tables 4 and 5, have been used to estimate the errors on our S abundances, as described in the next section.

Another systematic error is due to the microturbulent velocity. However, this is non-negligible only for the lines of Mult. 1, as the lines of Mult. 6 and 8 are weak and may be considered insensitive to microturbulence for all practical purposes. In fact, for a change of 0.5 km s^{-1}, the Monte Carlo simulation of 500 events shows a systematic error that is smaller than the random one.

In order to test the sensitivity of the lines of Mult. 1 to microturbulence, we performed a Monte Carlo simulation of 500 events and S/N = 150. The parameters of simulated observations were $T_{\rm eff}$ = 5800 K, log g = 4.25, [Fe/H] = −1.5, log(S/H) + 12 = 6.11, and ξ = 1.0 km s^{-1}. A run using synthetic spectra with the same parameters as the simulated observation (except for S abundance) provides A(S) = log(S/H) + 12 = 6.11 ± 0.08. If, in the same conditions, we use synthetic spectra with microturbulence of 1.5 km s^{-1} instead, we obtain A(S) = 6.05 ± 0.03. Therefore, an error of 0.5 km s^{-1} in the microturbulence results in an error of 0.06 dex in the S abundance. This systematic error is comparable to the random error. In Fig. 7 the variation of the residual intensity for a change of 0.5 km s^{-1} is shown.

A further source of systematic errors may be NLTE effects in these lines. Takada-Hidai et al. (2002) studied the NLTE effects for the lines of Mult. 6 and concluded that they are negligible. Chen et al. (2002) claim that the same must be true for the weaker lines of Mult. 8, which have the same low EP. Nissen et al. (2004) claim that NLTE should be small for the lines of Mult. 1 since, in their analysis, the S abundances derived from these lines agree with those derived from the lines of Mult. 6. The NLTE computations of Takada-Hidai et al. (2002) allow us to neglect NLTE effects with confidence for the lines of Mult. 6, the arguments of Chen et al. (2002) and Nissen et al. (2004) justify neglecting them for the lines of Mult. 1 and Mult. 8, although in these cases detailed NLTE computations would also be desirable. In particular, from our own analysis, the lines of Mult. 1 seem to provide S abundances which are about 0.17 dex higher than those derived from Mult. 8 and Mult. 6; this falls within the observational errors and may not be significant at all. However, it would be interesting to investigate possible NLTE effects. On this point see also the discussion in Ryde & Lambert (2004).

Finally, one should take the possible effects of granulation (Asplund 2004) into account. Such computations for these lines are not available at present, and we shall therefore ignore them, although we are aware that they might be relevant.

7. Sulphur abundances

The lines of Mult. 8 are not detectable for the most metal-poor stars in our sample. They are detected only in 28 out of 74 stars with a spectrum covering this spectral region, and the most metal-poor of them has [Fe/H] = −1.67.

Table 6. Radial velocity, atmospheric parameters and sulphur abundance.

Name	RV	$T_{\rm eff}$	$\log g$	[Fe/H]	Ref	$[S/Fe]_{670}$	$[S/Fe]_{870}$	$[S/Fe]_{920}$	[S/Fe]	[S/H]	σ
	km s^{-1}	K	cgs								
–09 122	–47	6087	4.16	–1.22	G03	<0.43	0.17	0.43	0.35	−0.84	0.11
–35 360	45	5048	4.53	–1.15	G03	<0.59	<0.59	0.54	0.54	−0.61	0.15
–61 282	221	5831	4.53	–1.25	G03	<0.69	0.63	0.66	0.64	−0.61	0.08
–68 74	–5	5757	4.01	–0.99	G03	0.47	0.36	0.30	0.35	−0.64	0.08
+02 263	–8	5754	4.87	–2.17	Apc	<1.08	<1.00	0.91	0.91	−1.26	0.14
–13 482	24	6194	4.34	–1.61	G96	–	0.33	0.32	0.32	−1.29	0.08
–69 109	61	5486	2.63	–0.95	G00	0.16	0.15	0.51	0.34	−0.61	0.06
+09 352	–64	6020	4.20	–2.09	Apc	–	–	0.34	0.34	−1.75	0.10
–60 545	11	5744	4.35	–0.82	G03	0.17	–	–	0.17	−0.65	0.12
+10 380	6	5739	4.12	–0.72	G03	0.31	–	–	0.31	−0.41	0.15
–09 6150	–33	5337	4.55	–0.63	G03	0.55	0.56	0.62	0.60	−0.03	0.08
+20 571	–117	5863	4.24	–0.83	N97	0.09	–	–	0.09	−0.74	0.14
–47 1087	11	5625	4.82	–0.79	G03	0.37	–	–	0.37	−0.42	0.13
–03 592	120	5827	4.33	–0.83	G03	0.14	–	–	0.14	−0.69	0.11
–26 1453	90	5900	4.37	–0.63	N97	0.21	–	–	0.21	−0.42	0.15
–57 806	55	5792	4.20	–0.91	G03	0.33	0.14	–	0.20	−0.71	0.08
–65 253	81	5351	4.57	–1.52	G03	–	<0.84	0.21	0.21	−1.31	0.10
–27 666	111	5970	4.45	–1.54	G03	<0.48	<0.48	0.40	0.40	−1.14	0.12
+05 824	–15	5897	4.33	–1.08	G03	0.26	–	–	0.26	−0.82	0.13
–59 1024	237	5894	4.49	–1.69	G03	<0.63	–	0.33	0.33	−1.36	0.09
+12 853	28	5388	4.62	–1.17	N97	<0.26	–	–	<0.26	<−0.91	0.14
–33 3337	71	6079	4.03	–1.28	G03	<0.62	–	–	<0.62	<−0.62	0.12
–57 1633	260	6013	4.34	–0.84	G03	<0.05	–	–	<0.05	<0.05	0.12
–45 3283	316	5692	4.82	–0.85	G03	<0.49	–	–	<0.49	<−0.36	0.14
G 88–40	–35	5967	4.26	–0.80	N97	0.18	–	–	0.18	−0.62	0.16
–15 2656	117	5923	4.14	–0.85	G03	0.12	–	–	0.12	−0.73	0.10
G 46–31	218	6021	4.44	–0.75	N97	<0.21	–	–	<0.21	<−0.54	0.18
–20 3540	167	6029	4.32	–0.79	N97	0.05	–	–	0.05	−0.74	0.12
–25 9024	120	5831	4.36	–0.80	N97	0.19	–	–	0.19	−0.61	0.13
G 12–21	100	6013	4.44	–1.27	G03	<0.68	–	–	<0.68	<−1.00	0.13
–09 3468	–5	6232	4.29	–0.72	G03	0.33	–	–	0.33	−0.39	0.12
+02 2538	155	6133	4.41	–1.69	G03	<0.56	<0.18	–	<0.18	<−1.55	0.09
–37 8363	226	5543	3.88	–0.70	G03	<0.34	–	–	<0.34	<−0.36	0.28
–38 8457	145	5964	4.32	–1.84	G03	–	0.66	–	0.66	−1.18	0.13
–56 5169	13	5383	4.57	–0.94	G03	<0.58	<0.36	–	<0.36	<−0.58	0.09
–45 8786	245	5686	4.40	–0.76	N97	0.29	0.24	–	0.26	−0.50	0.08
–17 4092	–46	5574	4.55	–1.14	G03	<0.41	<0.45	–	<0.41	<−0.73	0.08
–21 4009	176	5541	3.79	–1.67	G03	0.63	0.59	–	0.61	−1.06	0.07
+04 2969	18	5850	3.95	–0.84	G03	0.25	0.30	–	0.28	−0.56	0.07
–15 4042	310	4996	4.65	–1.38	G03	<0.39	<0.72	–	<0.39	<−0.99	0.11
–57 6303	9	4869	4.62	–1.39	G03	<0.83	–	–	<0.83	<−0.56	0.17
+06 3455	–136	5713	4.35	–0.84	G03	0.34	0.33	0.47	0.42	−0.42	0.08
+02 3375	–380	6018	4.20	–2.37	G96	–	–	0.34	0.34	−2.03	0.11
+05 3640	–1	5023	4.61	–1.19	G03	<0.93	<0.82	0.75	0.75	−0.44	0.15

Table 6. continued.

Name	RV	$T_{\rm eff}$	$\log g$	[Fe/H]	Ref	$[S/Fe]_{670}$	$[S/Fe]_{870}$	$[S/Fe]_{920}$	[S/Fe]	[S/H]	σ
	km s^{-1}	K	cgs								
–59 6824	–47	6070	4.17	–1.54	G03	<0.63	0.49	0.40	0.44	−1.11	0.09
+13 3683	86	5726	3.78	–2.43	Apc	–	–	0.47	0.47	−1.96	0.10
G 21–22	60	6123	4.28	–0.88	Apc	<−0.01	<−0.51	−0.14	−0.14	−1.02	0.11
–45 13178	30	5968	4.40	–1.81	G03	−−	0.84	–	0.84	−0.97	0.12
+10 4091	–193	5503	4.55	–1.45	G03	<0.55	<0.15	–	<0.15	<−1.30	0.09
–12 5613	–14	5668	3.79	–1.18	G03	<0.42	<0.40	–	<0.40	<−0.78	0.10
–21 5703	–173	5779	4.54	–1.09	G03	0.33	0.37	–	0.35	−0.74	0.09
+09 4529	–248	6023	4.31	–1.17	G03	<0.23	0.36	–	0.36	−0.81	0.13
–19 5889	–34	5893	4.12	–1.16	G03	0.36	0.44	0.56	0.50	−0.66	0.05
+04 4551	–117	5892	4.14	–1.40	G96	<0.54	<0.54	0.46	0.46	−0.94	0.14
+04 4674	–84	5772	4.03	–0.73	G03	0.24	0.26	0.56	0.42	−0.31	0.08
–28 17381	–105	5810	4.50	–1.16	G03	<0.50	<0.20	0.39	0.39	−0.77	0.13
+17 4708	–295	6016	4.04	–1.62	Apc	0.42	0.38	0.40	0.40	−1.22	0.07
+07 4841	–232	5980	4.00	–1.59	R88-P93	0.51	0.53	0.56	0.54	−1.05	0.08
HR 8515	31	5211	3.36	–1.56	G03	<0.75	<0.70	0.68	0.68	−0.88	0.16*
G 18–54	–217	5878	3.93	–1.33	Apc-P93	<0.07	<−0.01	−0.03	−0.03	−1.36	0.14*
–09 6149	–30	5756	4.26	–0.63	G03	0.45	0.44	0.69	0.57	−0.06	0.09
GD 660	–69	5712	4.50	–1.64	Apc	<1.09	<1.16	0.40	0.40	−1.24	0.17
GCRV 7547	–39	6272	4.03	–0.42	N97	0.04	–	–	0.04	−0.38	0.14
G 75 031	57	5884	4.24	–1.25	Apc	0.52	–	–	0.52	−0.73	0.14
–48 4818	–15	6503	4.11	–0.43	G03	>−0.18	–	–	>−0.18	>−0.61	0.18
–21 3420	6	5946	4.41	–1.04	N97	<0.45	–	–	<0.45	<−0.59	0.14

The column ("Ref") indicates the source of atmospheric parameter: G03: Gratton et al. (2003); N97: Nissen & Schuster (1997); P93: Pilachowski et al. (1993); Apc: Alonso, private comunication.
* Are SB2 stars, see Appendix A.

The stars for which we had a spectrum covering the lines of Mult. 6 were fewer, i.e. only the 50 stars with UVES spectra in common with Gratton et al. (2003). We derived sulphur abundances using the lines of Mult. 6 for 21 of them, the most metal-poor with [Fe/H] = −1.84.

Spectra covering the line range of Mult. 1 were available for 36 stars[4]. We detected these lines in 28 stars. In the remaining 8 stars we did not measure sulphur from the lines of Mult. 1 because the telluric lines blend all three lines of the multiplet, so their removal is unsatisfactory. The most metal-poor star in our sample has [Fe/H] = −2.43.

The concordance of the sulphur abundances deduced from the lines of Mult. 6 and Mult. 8. is generally good. There are 14 stars in which the lines of both multiplets were measured and the mean difference in [S/H] is 0.014 ± 0.06 (see Fig. 8).

No star has sulphur detection only in Mult. 8 and in Mult. 1. Five stars have sulphur detections in Mult. 6 and Mult. 8. Nine stars have sulphur detection in all three multiplets. For these 9 stars, we plot the mean [S/H] measured from Mult. 6 and Mult. 8 versus the value measured from Mult. 1 in Fig. 8.

[4] A slightly different setting was used in the different runs of programme 165.L-0263 and the setting used in the first run did not cover the region of the S I Mult. 1 lines.

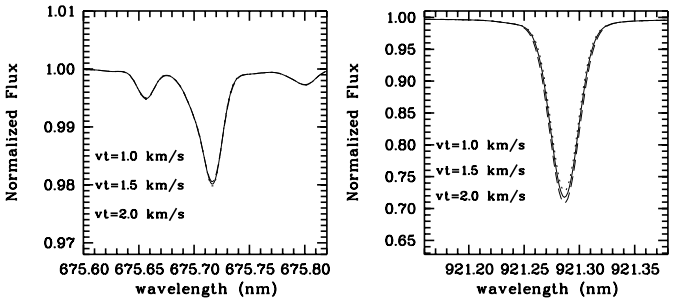

Fig. 7. Microturbulence effect on sulphur lines; the synthetic spectra plotted have: $T_{\rm eff}$ = 5810 K, $\log g$ = 4.50, [Fe/H] = −1.0, which are the parameters of the star HD 205650. This star has been selected to show microturbulence effect, because its parameters fall near the average of our sample.

A simple regression provides a slope of 1.07 (±0.15) and an offset of 0.18 (±0.11) dex. Due to the size of the errors, it is not clear whether this offset is significant. We tested this effect by applying it to all the measurements from Mult. 1, but none of our conclusions is affected by it. We therefore decided not to apply this small and uncertain correction to our measurements. The two stars which show the largest discrepancy, greater than 0.3 dex, are HD 17072 and HD 204155. HD 17072

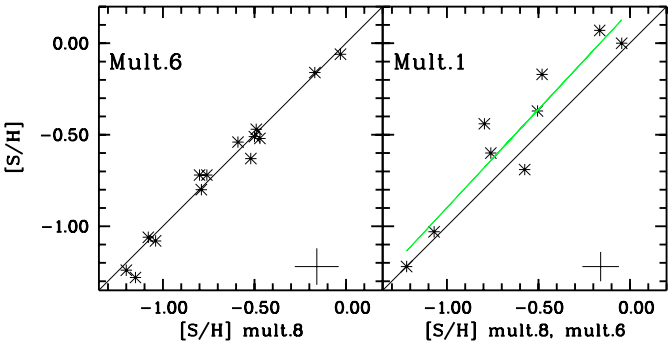

Fig. 8. *Left*: [S/H] derived from the lines of Mult. 6 versus [S/H] derived from the lines of Mult. 8 for all the stars with measurements in both multiplets. *Right*: [S/H] derived from the lines of Mult. 1 versus mean [S/H] derived from the lines of Mult. 8 and Mult. 6 for all the stars with measurements in all three multiplets. In both plots the solid line is the bisector; the cross at bottom is a representative error bar. The bisector shows the good agreement of [S/H] between Mult. 8 and Mult. 6 (*left*). The systematic difference of [S/H] derived from Mult. 1 is shown by the linear correlation (grey line).

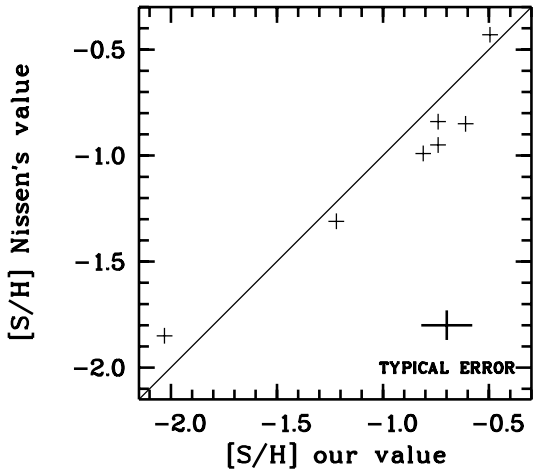

Fig. 9. Comparison of [S/H] value from our measurements and the determination of Nissen et al. (2004).

is the only giant star in our sample with a microturbulent velocity of 2.1 km s^{-1} (Carney et al. 1994). HD 204155 is a dwarf with a microturbulent velocity of 0.98 km s^{-1} (Gratton et al. 2003). For both stars the S abundance deduced from the lines of multiplets 6 and 8 are in excellent agreement. In both cases an increase of the microturbulent velocity on the order of 1 km s^{-1} would bring the S abundance deduced from the lines of Mult. 1 in agreement with that deduced from the other lines, but we have no justification for such an increase.

The tenth column in Table 6 provides the final adopted value of [S/Fe] for each star, which is simply the mean of the measurements we made, and the last one is the associated error. There are 50 stars with an [S/H] determination. We could not determine sulphur abundances for all the stars in the sample, but we give some upper limits. For some stars, no determination or upper limit was possible either because of bad pixels, or because the signal-to-noise ratio was too low. For one star (HD 83220), we give a lower limit because a cosmic ray lies on the core of the sulphur line (675.7 nm), which is clearly present. In those cases for which upper limits were available for some lines and detections for others, we ignored the upper limits.

To compute an error estimate for our sulphur measurements, we used the *S/N* ratios given in Table A.1, and used the results of the Monte Carlo simulations in Table 4 to estimate the random error which was added linearly to the systematic errors due to $T_{\rm eff}$ and log g errors, as discussed in the previous section. Finally, the result was divided by $\sqrt{n}$, where n is the number of multiplets for which we have an S measurement. Errors on upper limits were computed in the same way, but only for the stars for which we have no measures. Our error estimates for [S/H] are provided in the last column of Table 6.

7.1. Comparison with other authors

We share few stars with other authors: one star (HD 194598) is in common with Israelian & Rebolo (2001) and [S/H] is in good agreement (difference = 0.04 dex); one star (HD 22879) is in common with Chen et al. (2003) with [S/H] in good agreement (difference of 0.01 dex); 7 stars are in common with Nissen et al. (2004), the mean difference is +0.08 ± 0.15, with no evidence of any systematic effect (see Fig. 9).

8. Results

Our sample is probably too small to adequately investigate the evolution of sulphur abundances. It is, therefore, worthwhile to combine our sample with the other measures available in the literature. Since there is little overlap among the different samples in the literature, it is possible to gain considerable insight by combining them. We took the data from Israelian & Rebolo (2001), Takada-Hidai et al. (2002), Chen et al. (2002), Chen et al. (2003), Ryde & Lambert (2004), Nissen et al. (2004), and Ecuvillon et al. (2004) and combined them with our own. We considered the log gf values used by the different authors and concluded that all the above S measurements are on the same scale, since the differences in adopted log gf are usually smaller than the abundance errors (see Sect. 4.2). When a star was observed by several authors, we proceeded as follows: if the star was also in our own sample we kept our measurements; if different authors adopted similar atmospheric parameters we took a straight average of the different measurements; if, instead, the adopted atmospheric parameters were significantly different, we adopted only one of the measurements according to our perception of which was the most reliable. For example, for the stars common to Chen et al. (2002) and Nissen et al. (2004), we preferred Nissen et al. (2004), since most likely VLT data are of higher quality, and so on. This procedure is somewhat arbitrary, but is preferable to taking a straight average of S abundances derived by adopting different effective temperatures. Moreover, this regards a very limited number of stars, and the general conclusions we derive do not depend on these choices. In this way we assembled a sample of 253 stars with a unique [S/H] value, and this compilation is given in Table A.2. The overlap among the different investigations is minimal: only 29 stars are analyzed by more than one author. In Col. 11 of Table A.2 we

provide the reference to all the papers which provide S measurement for a given star.

The data of Israelian & Rebolo (2001) and Ryde & Lambert (2004) are not in agreement, even if they use the same $T_{\rm eff}$. We adopted the mean value. The two authors considered two different regions: Israelian & Rebolo (2001) used the lines of Mult. 6, while Ryde & Lambert (2004) used the lines of Mult. 1. We note that sulphur abundances in Ryde & Lambert (2004) are systematically lower than those in Israelian & Rebolo (2001).

HD 9826 presents a different sulphur abundance in (Chen et al. 2002, +0.16) and in (Ecuvillon et al. 2004, –0.20), even if the same lines are considered in the two papers. HD 217107 presents the same problem.

9. Discussion

9.1. The behaviour of sulphur versus iron

In Fig. 10 (bottom panel) we show the usual [S/Fe] versus [Fe/H] plot, which displays a very clear rise of [S/Fe] from solar metallicity up to [Fe/H] ~ -1 and then a rather large scatter. It is also interesting to consider the plot of [S/H] versus [Fe/H] (Fig. 10, top panel). This shows a clear correlation between the abundances of the two elements. There is, however, a very clear break in the slope around [Fe/H] ~ -1, and also in this case the larger scatter at lower metallicities is obvious. Another intriguing feature is that, while at low metallicities [Mg/Fe] (see Fig. 16) seems to be essentially flat, in Fig. 10 for [S/Fe] there is a group of stars which seems to display a very clear linear increasing trend, as claimed by Israelian & Rebolo (2001) and Takada-Hidai et al. (2002), and another group which seems to display a constant [S/Fe], as found by Chen et al. (2002, 2003); Ryde & Lambert (2004); Nissen et al. (2004).

The increase of [S/Fe] with decreasing metallicity, already highlighted by previous investigations, is obvious. However, there are a few features, which are not obvious when taking each data set separately, that stand out once all the data are assembled together as in Fig. 10:

1. around [Fe/H] ~ -1 there is a sizeable spread in [Fe/H], clearly larger than at higher metallicities;
2. for lower metallicities the spread increases with decreasing [Fe/H] and there is in fact a hint of bimodality. Some stars have "high" [S/Fe], which continues to increase, other stars have "low" [S/Fe] which display a "plateau".

Before attempting to understand the origin of these features, it is necessary to assess if it is astrophysical or if they are originated by observational bias or errors.

For the first feature one could presume that the metallicity bin around [Fe/H] ~ -1 is the most populated, since stars of this metallicity are included both in samples consisting mainly of metal-poor stars and in samples consisting mainly of more metal-rich stars. The observational scatter, added to the different systematics of the different investigations, may give rise to this excess of scatter. Although this possibility cannot be ruled out and indeed most certainly contributes to increase the existing scatter, we point out that the feature seems to exist both in our own data and in the data of Nissen et al. (2004), albeit in either sample it is less clear, due to small number statistics. We are thus inclined to consider this feature to be of astrophysical origin.

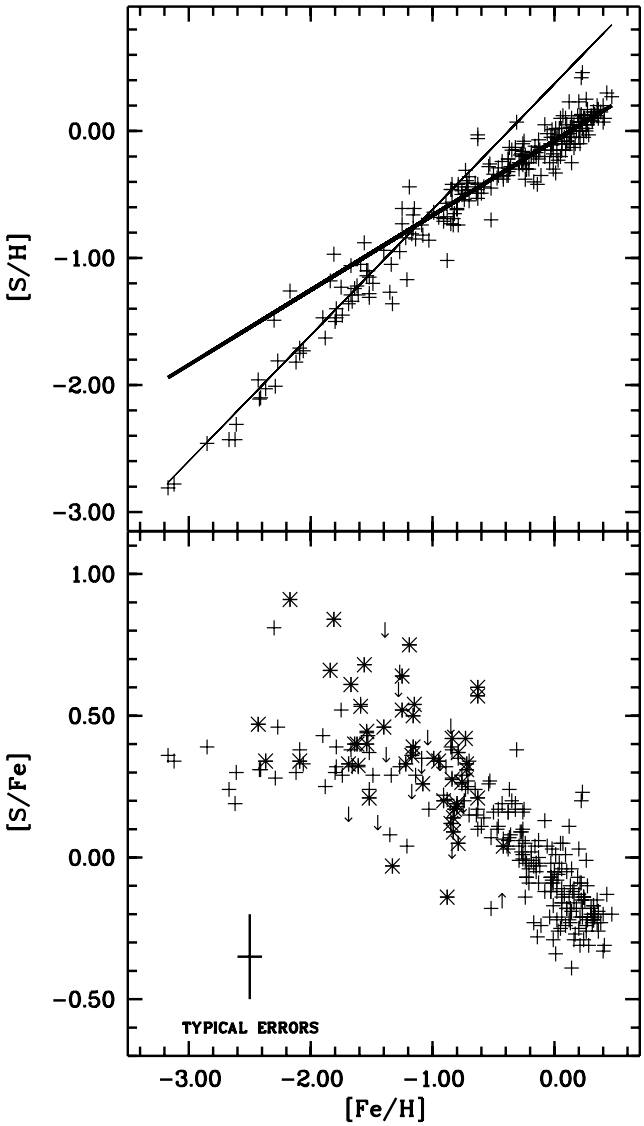

Fig. 10. *Bottom panel*: [S/Fe] versus [Fe/H]. The measures of the present paper are indicated as asterisks, crosses are the data taken from the literature (Table A.2). The typical error bar is shown in the lower left corner. *Top panel*: [S/H] versus [Fe/H] for all stars considered. Two different linear trends can be distinguished: the thick line is a fit to all stars with [Fe/H] > -1, the thin line to those with [Fe/H] ≤ -1.0.

The second feature is apparent in this work for the first time. It was well known that the works of Israelian & Rebolo (2001) and Nissen et al. (2004) were in disagreement. The first displays a steady increase of [S/Fe] with metallicity and the second a clear "plateau", but researchers in the field were inclined to believe that either set was plagued by some undetected systematic effect and thus should be discarded. Very intriguingly, our own results are in good agreement with the trend of Israelian & Rebolo (2001) and Takada-Hidai et al. (2002) for some stars and with that of Nissen et al. (2004) for some other stars, giving support to the idea that either at low metallicity there is a large scatter in S abundances, or there are two

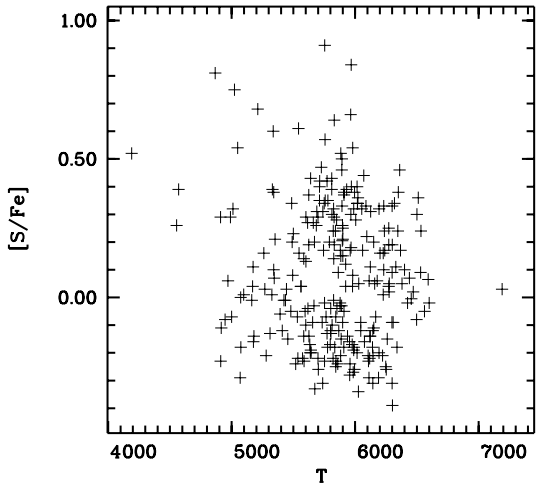

Fig. 11. The [S/Fe] ratio versus effective temperature for all the stars in Table A.2. No trend is discernible.

distinct populations, one with an increasing [S/Fe] with decreasing metallicity and the other one with a "plateau". A possible cause of concern is that all the data at low metallicity, where this behaviour becomes apparent, rely exclusively on the lines of Mult. 1 ($4s-4p^5S^\circ-^5P$) because the other lines are vanishingly small. If, for example, these lines were affected by significant NLTE effects one would expect this to be stronger for hotter stars, thus causing the observed scatter. However, this cannot be the case, since in our own sample the ranges in temperature and gravity, spanned by the stars with "high" [S/Fe] and "low" [S/Fe], are the same. Again, the temperature range spanned by the stars of Israelian & Rebolo (2001) is comparable to that spanned by the stars of Nissen et al. (2004), so stars with "high" [S/Fe] do not seem to be systematically different from stars with "low" [S/Fe]. We checked if there is any dependence of the [S/Fe] ratio on effective temperature or gravity, in order to highlight any possible systematic error, but we found none. In Fig. 11 we show the [S/Fe] ratios versus $T_{\rm eff}$ for all stars, and there appears to be no trend, as could be expected if NLTE effects on the lines of Mult. 1 were important. In Fig. 12 we show the fit on the 921.2 nm line of Mult. 1 for four stars from our sample: all the fits are good and, therefore, unless we overlooked some systematic effect, the deduced abundances should be reliable.

The substantial agreement between our sulphur abundances and those of Nissen et al. (2004) for the stars in common militates against the idea of any systematic difference between the two analysies.

After studying the works of Nissen et al. (2004) and Israelian & Rebolo (2001) carefully, we conclude that the only possible systematic difference is that Nissen et al. (2004) subtracted the telluric lines, while Israelian & Rebolo (2001) included only stars for which at least one line was measurable.

9.2. Kinematic properties

In order to classify the stars on the basis of their kinematics, we computed space velocities for all the stars for which

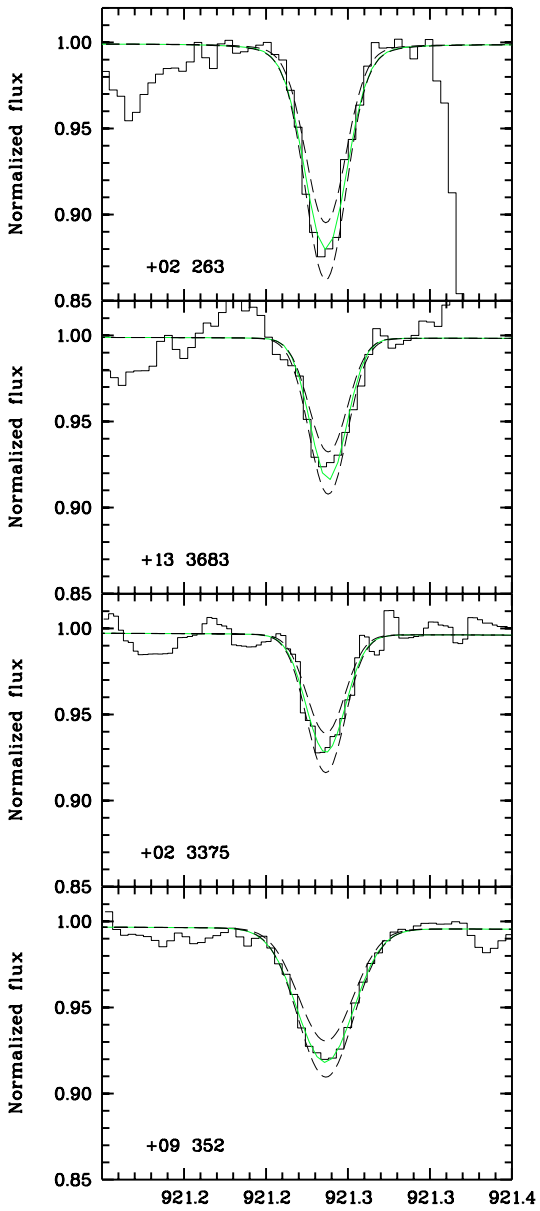

Fig. 12. Fit of the 921.2 nm line (grey line) of four of the most metal poor stars that lie in different places in the plot [S/Fe] versus [Fe/H]. Dashed lines are synthetic spectra computed with ±0.1 dex the best fitting abundance. As one can see the four fits are good, and the abundance deduced by these fits should be reliable.

parallaxes and proper motions are available from the Hipparcos or Tycho catalogues (Perryman et al. 1997). When available radial velocities were taken from our own measurements, or from Nordström et al. (2004), or, in sequence, Latham et al. (2002) or Beers et al. (2000). When no other data were availabe the radial velocity in Simbad was used. To transform radial velocities and proper motions into space velocities, we used the transformation matrices of Johnson & Soderblom (1987), except that we adopted a left-handed coordinate system with U directed towards the Galactic anticentre, V in the direction of Galactic rotation and W towards the North Galactic Pole. The kinematic data for the stars are given in Table A.2. In Fig. 10 there is a group of 15 stars with [S/Fe] > 0.48, which seem to follow a

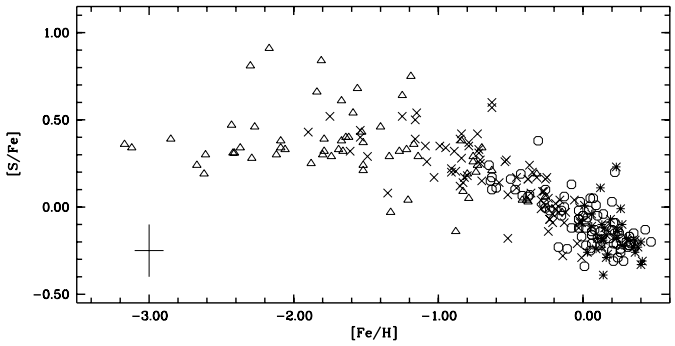

Fig. 13. [S/Fe] versus [Fe/H] for the stars classified on the basis of their Galactic orbits: open circles are the thin disc stars, crosses the dissipative component, triangles the accretion component, and the asterisks are the stars which do not fall in any of these categories.

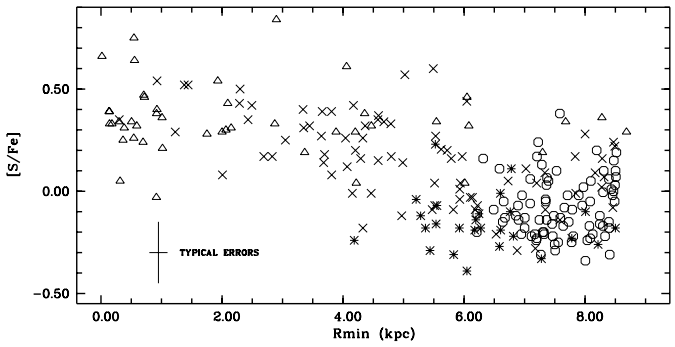

Fig. 14. [S/Fe] as a function of perigalactic distance Rmin, in kpc. The different populations are marked as in Fig. 13.

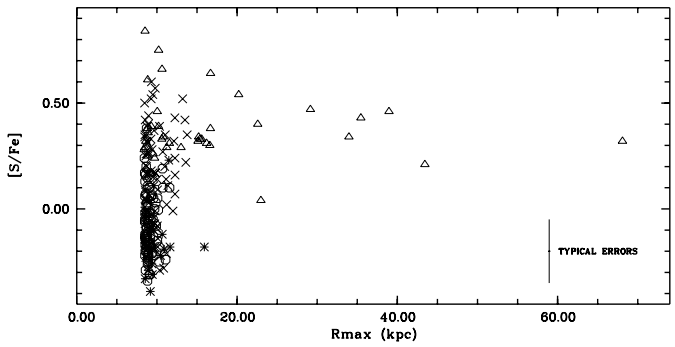

Fig. 15. [S/Fe] as a function of apogalactic distance Rmax, in kpc. The different populations are distinguished as in Fig. 13.

different trend from the other stars. We inspected various kinematical properties: the Toomre velocity ($T = \sqrt{U^2 + W^2}$), the speed ($S = \sqrt{U^2 + V^2 + W^2}$), the rotational velocity. However, this group of stars does not appear to have any kinematical property distinct from the other ones.

With the velocity and position data, we integrated the orbits in the same way as done in Gratton et al. (2003), and the resulting orbital parameters are reported in Table A.2. We used these data to classify the stars into *thin disc*, *dissipative component*, and *accretion component* using the same criteria as Gratton et al. (2003). We note four stars which have apogalactic distances above 100 kpc and extremely high eccentricities, which could be in fact runaway stars on parabolic orbits, and

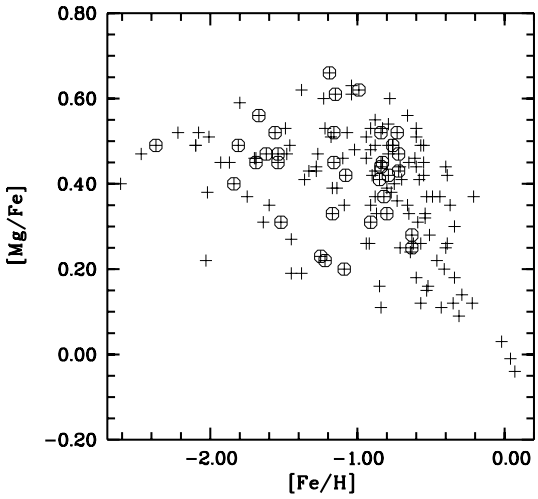

Fig. 16. [Mg/Fe] versus [Fe/H] from Gratton et al. (2003); circled stars are those in common with the present study.

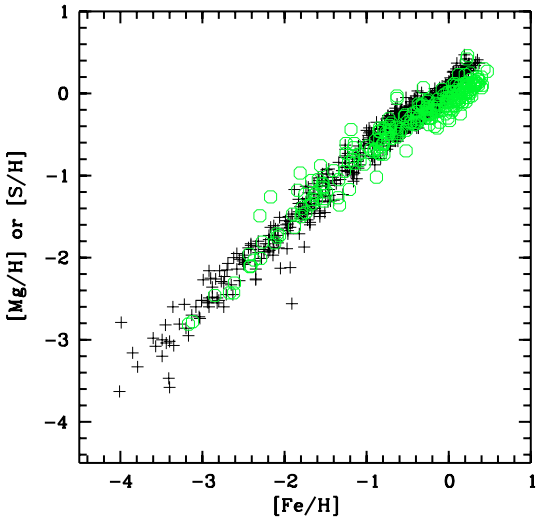

Fig. 17. [Mg/H] versus [Fe/H] for the stars in the compilation of Venn et al. (2004) (crosses) and [S/H] versus [Fe/H] (open hexagons) from the compilation in Table A.2.

all four are classified as belonging to the accretion component. Not surprisingly, two of them are the well known extremely metal-poor dwarfs G64-12 and G64-37; the other two are intermediate metallicity stars HD 105004 and G53-41.

From Fig. 13 we see that we find both "high" [S/Fe] stars and "low" [S/Fe] stars among the dissipative component, as well as among the accretion component. On average the thin disc stars have lower [S/Fe] ratios and higher metallicities. The dissipative component also seems to show a larger scatter in [S/Fe] ratios than either of the other populations. In Fig. 15 [S/Fe] is shown as a function of apogalactic distance; and although on average stars with Rmax larger than 15 kpc appear to have higher [S/Fe] ratios, there are some exceptions. Moreover, there does not seem to be any preferred range of Rmax for any given range in [S/Fe]. From Fig. 14 one may note a very clear trend of increasing [S/Fe] with decreasing perigalactic distance; on average, the stars which penetrate closer to the Galactic centre display higher [S/Fe] ratios. Kendall's τ test

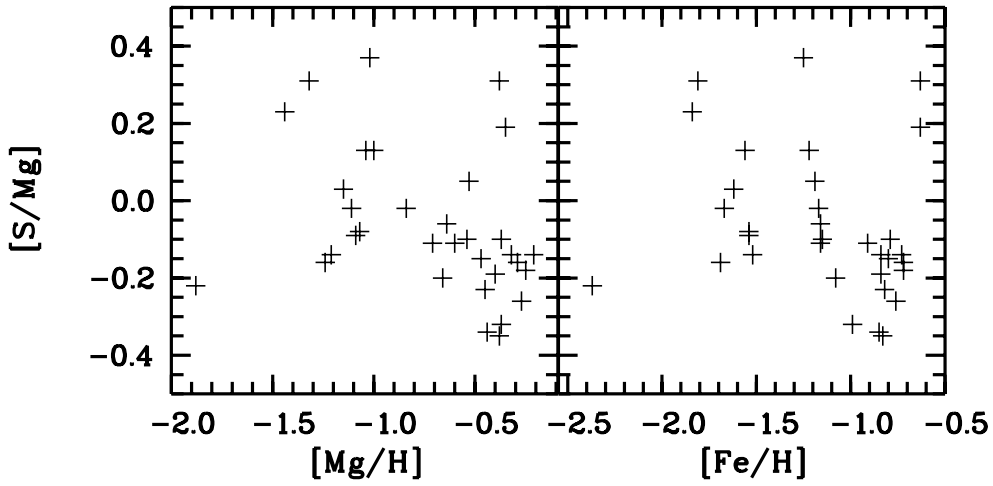

Fig. 18. [S/Mg] versus [Mg/H] (*left panel*) and [Fe/H] (*right panel*). Mg abundances are from Gratton et al. (2003).

confirms the reality of this correlation with a probability close to 1 ($1-prob \sim 4\times10^{-19}$). However, if we consider the different populations separately, we conclude that neither the accretion component nor the thin disc displays any trend of [S/Fe] versus Rmax, and it is only the dissipative component which displays this trend.

Thus the dissipative component is in qualitative agreement with the theoretical results of Fenner et al. (2004), who predict that at any metallicity the [S/Fe] ratio should be higher for stars in the inner disc (discussion in Sect. 9.3). The thin disc, instead, is not in agreement with this prediction.

9.3. The behaviour of sulphur with magnesium and zinc

It is instructive to compare our data for sulphur with the data for another α element, so we took magnesium from Gratton et al. (2003). The situation for silicon is essentially the same. The data are displayed in Fig. 16. At first sight the plot seems very similar to the lower panel of Fig. 10; however, a closer inspection reveals that while for Mg for any given [Fe/H], the [Mg/Fe] value spans a range of 0.3–0.4 dex, the range can be as large as 0.7 dex for [S/Fe]. In Fig. 17 we show [Mg/H] versus [Fe/H] for 725 Galactic stars from the compilation of Venn et al. (2004) as crosses overlaid on [S/H] from the data in Table A.2 (open circles). This comparison highlights two differences in the behaviour of the two elements: 1) the break of slope at [Fe/H] ~ -1 is more pronounced for sulphur than magnesium, the latter displaying a steeper slope in the high metallicity range; 2) the width of the strip in sulphur is wider than in magnesium, in particular the eye easily detects a locus of stars with higher [S/H] for a given [Fe/H], whereas such a locus is not present for [Mg/H] data.

For the the sub-sample of our programme stars shared with Gratton et al. (2003) we may directly form ratios of sulphur with other elemental abundances, since the atmospheric parameters are the same. In particular, in Fig. 18 we show the ratios [S/Mg] both as a function of [Mg/H] (left panel) and [Fe/H] (right panel). From this plot a large scatter in the S/Mg ratios is apparent, with a hint of a trend of ratios increasing with decreasing metallicities. This suggests that sulphur and magnesium do not vary in lockstep in the Galactic evolution, although the sample is too small and the errors too large to reach a definitive conclusion.

In Fig. 19, instead, we show the [S/Zn] ratios as a function of [Zn/H]. Morphologically this plot is similar to the one in Fig. 18, although the metallicity range appears more compressed. This figure is interesting for many reasons. Zinc has been the object of several studies in Damped Lyman α (DLA) galaxies (Pettini et al. 1994, 1997; Centurión et al. 2000; Nissen et al. 2004). With respect to other pairs of elements, zinc and sulphur have the advantage that both are volatile, i.e. form no dust in the warm interstellar medium (Savage & Sembach 1996), so that the nucleosynthetic implications of the observed ratios may be investigated in DLAs without the need to use uncertain dust corrections. There is an ongoing debate on whether the S/Zn may actually be used as a proxy for α/Fe (Centurión et al. 2000) or not (Prochaska et al. 2000; Fenner et al. 2004).

From a theoretical point of view, Fe and Zn should behave differently because Fe is abundantly produced by Type Ia SNe, while Zn should not (Iwamoto et al. 1999). However, Matteucci et al. (1997) have invoked a Zn production by Type Ia SNe in order to explain the flatness of the Zn/Fe ratio in Galactic stars (see Gratton et al. 2003). Without invoking this ad hoc production, Fenner et al. (2004) have shown that for a model of a Milky Way-like galaxy the evolution of the [S/Fe] ratios is different at different galactocentric radii, due to the different star formation rates. However, [S/Zn] should behave in a very similar manner at all galactocentric radii (see Fig. 7 of Fenner et al. 2004). It would be tempting to interpret the large scatter in S/Fe ratios in our data as the result of sampling stars which have evolved at different Galactocentric radii, at least for the dissipative component, which shows a clear trend of [S/Fe] with Rmin (see Fig. 14). However, it should be noted that the orbits of the dissipative component display a wide range of eccentricities and the difference between Rmax and Rmin has a mean value of ∼5 Kpc. Therefore these stars span a significant range of Galactocentric radii, and it may not be appropriate to think they represent the chemical evolution at a "typical Galactocentric

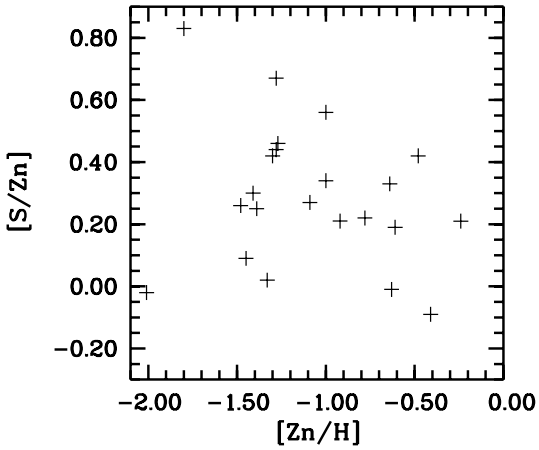

Fig. 19. [S/Zn] versus [Zn/H]. Zn abundances are from Gratton et al. (2003).

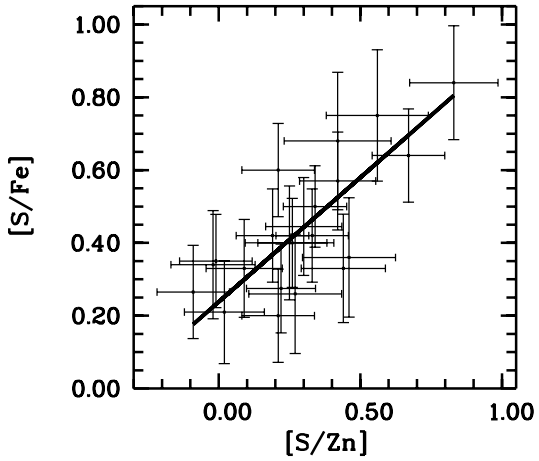

Fig. 20. [S/Fe] versus [S/Zn]. Zn abundances are from Gratton et al. (2003). The solid line is a least squares fit to the data: [S/Fe] = 0.68 [S/Zn]+0.24.

radius". Note also that, theoretically, the difference in [S/Fe] between inner and outer disc ought to be on the order of 0.2 dex, while the spread in our data is as large as 0.6 dex. In Fig. 20 we show [S/Fe] versus [S/Zn] for the 22 stars for which we have measurements of both sulphur and zinc. There is a clear correlation between the two, and a linear least squares fit, taking errors in both variables into account, is shown as a solid line: [S/Fe] = 0.68[S/Zn] + 0.24. These data therefore suggest that [S/Zn] may be used as a proxy of [S/Fe], contrary to the predictions of the model of Fenner et al. (2004). One should, however, keep in mind that this result rests on sulphur and zinc abundances for only 22 stars.

10. Conclusions

In the light of the current observations, we conclude that both stars with [S/Fe] $\sim$ 0.4 and with higher [S/Fe] ratios exist at the metal-poor end of the metallicity distribution of Galactic stars. We have not been able to ascertain whether this reflects a larger scatter in sulphur abundances at low metallicities or the existence of two distinct populations.

Acknowledgements. E.C. and P.B. are grateful to Miguel Chavez for useful discussions on the topic of stellar abundances and for his hospitality at the INAOE, where a considerable part of this work was carried out. We wish to thank Harri Lindgren for providing unpublished periods for HD 83220 and HD 106516. Finally special thanks are due to Gabriella Schiulaz for helping us to refurbish our language.

References

Anders, E., & Grevesse, N. 1989, Geochim. Cosmochim. Acta, 53, 197
Asplund, M. 2004, MSAIt, 75, 300
Bashkin, S., & Stoner, J. O. 1978 (Amsterdam: North-Holland Publ. Co.)
Beers, T. C., Chiba, M., Yoshii, Y., et al. 2000, AJ, 119, 2866
Biemont, E., Quinet, P., & Zeippen, C. J. 1993, A&AS, 102, 435
Bonifacio, P., & Caffau, E. 2003, A&A, 399, 1183
Carney, B. W., Latham, D. W., Laird, J. B., & Aguilar, L. A. 1994, AJ, 107, 2240
Castelli, F., & Kurucz, R. L. 2004, [arXiv:astro-ph/0405087]
Centurión, M., Bonifacio, P., Molaro, P., & Vladilo, G. 2000, ApJ, 536, 540
Chen, Y. Q., Nissen, P. E., Benoni, T., & Zhao, G. 2001, A&A, 371, 943
Chen, Y. Q., Nissen, P. E., Zhao, G., & Asplund, M. 2002, A&A, 390, 225
Chen, Y. Q., Zhao, G., Nissen, P. E., Bai, G. S., & Qiu, H. M. 2003, ApJ, 591, 925
Clegg, R. E. S., Tomkin, J., & Lambert, D. L. 1981, ApJ, 250, 262
Ecuvillon, A., Israelian, G., Santos, N. C., et al. 2004, A&A, 426, 619
Fenner, Y., Prochaska, J. X., & Gibson, B. K. 2004, ApJ, 606, 116
François, P. 1987, A&A, 176, 294
François, P. 1988, A&A, 195, 226
Fuhrmann, K., & Bernkopf, J. 1999, A&A, 347, 897
Garnett, D. R. 1989, ApJ, 345, 282
Gratton, R. G. 1998, MNRAS, 296, 739
Gratton, R. G., Carretta, E., Claudi, R., Lucatello, S., & Barbieri, M. 2003, A&A, 404, 187
Gray, R. O. 1989, AJ, 98, 1049
Grevesse, N., Noels, A., & Sauval, A. J. 1996, Cosmic Abundances, ASP Conf. Ser., 99, 117
Grevesse, N., & Sauval, A. J. 1998, Space Sci. Rev., 85, 161
Hartkopf, W. I., Mason, B. D., & Wycoff, G. L. 2004, Fourth Catalog of Interferometric Measurements of Binary Stars, http://ad.usno.navy.mil/wds/int4.html
Israelian, G., & Rebolo, R. 2001, A&A, 557, L43
Iwamoto, K., Brachwitz, F., Nomoto, K., et al. 1999, ApJS, 125, 439
James, F. 1998, MINUIT, Reference Manual, Version 94.1, CERN, Geneva, Switzerland
Johnson H. R., & Kinglesmith, D. A. 1965, in Harvard-Smithsonian Conference on Stellar Atmospheres, Proc. of the Second Conference, SAO Spec. Rep. 174, Cambridge Smithsonian Astrophysical Observatory, 246
Johnson, D. R. H., & Soderblom, D. R. 1987, AJ, 93, 864
Kurucz, R. L., Furenlid, I., & Brault, J. T. L. 1984, National Solar Observatory Atlas, Sunspot, New Mexico: National Solar Observatory
Kurucz, R. L. 1993, CD-ROM 13, 18 http://kurucz.harvard.edu
Lambert, D. L., & Warner, B. 1968, MNRAS, 138, 181
Lambert, D. L., & Luck, R. E. 1978, MNRAS, 183, 79
Lambert, D. L., & McWilliam, A. 1986, ApJ, 304, 436
Latham, D. W., Stefanik, R. P., Torres, G., et al. 2002, AJ, 124, 1144

Limongi, M., & Chieffi, A. 2003, MSAIS, 3, 58
Lindgren, H., Ardeberg, A., & Zuiderwijk, E. 1989, A&A, 218, 111
Lodders, K. 2003, ApJ, 591, 1220
Malaroda, S. 1973, PASP, 85, 328
Malaroda, S. 1975, AJ, 80, 637
Matteucci, F., Molaro, P., & Vladilo, G. 1997, A&A, 321, 45
Maurice, E., Spite, F., & Spite, M. 1984, A&A, 132, 278
Molaro, P., Bonifacio, P., Castelli, F., & Pasquini, L. 1997, A&A, 319, 593
Moore, C. E. 1972, A multiplet table of astrophysical interest NSRDS-NBS (Washington: US Department of Commerce), Rev. edition
Moore, C. E., Minnaert, M. G. J., & Houtgast, J. 1966, The solar spectrum 2935 Å to 8770 Å, National Bureau of Standards Monograph (Washington: US Government Printing Office, USGPO)
Nissen, P. E., & Schuster, W. J. 1997, A&A, 326, 751
Nissen, P. E., Chen, Y. Q., Schuster, W. J., & Zhao, G. 2000, A&A, 353, 722
Nissen, P. E., Chen, Y. Q., Asplund, M., & Pettini, M. 2004, A&A, 415, 993
Nordström, B., Mayor, M., Andersen, J., et al. 2004, A&A, 418, 989
Perryman, M. A. C., & ESA 1997, The Hipparcos and Tycho catalogues, Astrometric and photometric star catalogues derived from the ESA Hipparcos Space Astrometry Mission (Noordwijk, Netherlands: ESA Publications Division), ESA SP Ser., 1200
Peterson, R. C., Carney, B. W., Dorman, B., et al. 2003, ApJ, 588, 299
Pettini, M., Smith, L. J., Hunstead, R. W., & King, D. L. 1994, ApJ, 426, 79
Pettini, M., Smith, L. J., King, D. L., & Hunstead, R. W. 1997, ApJ, 486, 665
Pilachowski, C. A., Sneden, C., & Booth, J. 1993, ApJ, 407, 699
Press, W. H., Teukolsky, S. A., Vetterling, W. T., & Flannery, B. P. 1992 (Cambridge: University Press), 2nd edn.
Prochaska, J. X., Naumov, S. O., Carney, B. W., McWilliam, A., & Wolfe, A. M. 2000, AJ, 120, 2513
Ryde, N., & Lambert, D. L. 2004, A&A, 415, 559
Sansonetti, J. E., & Martin, W. C. 2004, Handbook of Basic Atomic Spectroscopic Data, http://physics.nist.gov/PhysRefData/Handbook/index.html
Savage, B. D., & Sembach, K. R. 1996, ARA&A, 34, 279
Sbordone, L., Bonifacio, P., Castelli, F., & Kurucz, R. L. 2004, MSAIS, 5, 93
Takada-Hidai, M., Takeda, Y., Sato, S., et al. 2002, ApJ, 573, 614
Torres-Peimbert, S., Peimbert, M., & Fierro, J. 1989, ApJ, 345, 186
Venn, K. A., Irwin, M., Shetrone, M. D., et al. 2004, AJ, 128, 1177
Wiese, W. L., Smith, M. W., & Miles, B. M. 1969, NSRDS-NBS (Washington, D.C.: US Department of Commerce), National Bureau of Standards

Online Material

Appendix A: Remarks on individual stars

1. HD 3567: the difference between the determination of sulphur abundance from the lines of Mult. 6 and that from those of Mult. 1 is not explained; it may be due to weakness of the Mult. 6 lines.
2. HD 17072: the star is an RHB according to Carney et al. (1994). Gratton (1998) notes that it may be on the first ascent of the giant branch rather than on the horizontal branch. The incoherent sulphur abundance in the three regions remains unexplained. For Mult. 1 the good fit is based on two lines, while the third one was discarded for its contamination by a telluric line; the slight contamination by telluric of the two considered lines was easily removed. Sulphur abundance for Mult. 8 and 6 is based on one sulphur line for each multiplet. We note that a broadening higher than the instrumental resolution is required; the microturbulence of 2.1 km s^{-1} from Carney et al. (1994) was adopted.
3. G 76 –21: it has peculiar line profiles. The lines appear broad (higher than instrumental resolution) with a flat and double core (see Fig. A.1). Carney et al. (1994) suspected it of being a double-lined system; the duplicity is not confirmed by Latham et al. (2002), who measured only a small amplitude variation for radial velocity.
4. HD 83220: this star presents broad lines. The rotational velocity (9 km s^{-1}) of Nordström et al. (2004) is the highest in the sample of stars in common with ours. This star is a spetroscopic binary for which Lindgren (private communication) determined a preliminary orbit with a period of 765.8 days.
5. HD 103723 and HD 105004: the low α-enhancement found by Nissen et al. (2004) is not evident from our spectra. Both stars are suspected binares from Hipparcos data: HD 103723 is D (duplicity induced variability); HD 105004 is S (suspected not single) and X (probably an astrometric binary with short period).
6. HD 106038: we suspect the star is double. We recall the peculiar abundances found by Nissen & Schuster (1997), but not by Chen et al. (2001).
7. HD 106516: a spectroscopic binary. Latham et al. (2002) give a period of 853.2 d, and Lindgren (private comunication) a period of 841 d. It is one of the few stars presenting lines broader than instrumental resolution in agreement with Nordström et al. (2004) who give $v \sin i$ = 8 km s^{-1}. Peterson et al. (2003) establish it as a halo blue straggler, which had already been suggested by Fuhrmann & Bernkopf (1999) based on the unexpectedely high projected rotational velocity. Its blue straggler nature may in fact explain the absence of detectable Be in its atmosphere (Molaro et al. 1997).
8. HD 113083: we observe the duplicity discovered by Lindgren et al. (1989) and confirmed by Nissen & Schuster (1997) and by Nissen et al. (2000). HD 113083 is an SB2 with nearly identical sets of lines; see Nissen & Schuster (1997) for the resolved system parameters and abundances.
9. HD 132475: we note the disagreement between the temperature adopted by us (5541 K) and the one adopted by (Ryde & Lambert 2004, 5810 K). The synthetic spectrum computed with the temperature adopted by us fits the observed H_α better than the one computed with the $T_{\rm eff}$ used by Ryde & Lambert (2004).
10. HD 204155: we note a large difference of the value of the sulphur abundance from Mult. 8 and 6 with respect to that derived from Mult. 1. No signs of duplicity can be deduced from the radial velocity data of Latham et al. (2002) covering more than 3000 days.
11. HD 211998: only the 921.28 nm line of Mult. 1 was detected. The H_α profile is not in good agreement with the synthetic spectrum. In spite of being a much studied bright star (V = 5.29), its duplicity is questionable. Malaroda (1973) and Malaroda (1975) classified it as a spectroscopic binary composed of an A and an F star. Gray (1989) suspected it of having a composite spectrum. However, Lambert & McWilliam (1986) discarded the duplicity hypothesis.
    The presence of Li (Maurice et al. 1984) but not Be (Molaro et al. 1997), is at odds with predictions of standard stellar evolution theory.
    Hipparcos (Perryman et al. 1997) did not detect any companion and the speckle measurements (Hartkopf et al. 2004) are uncertain.
12. G 18–54: sulphur was detected only for Mult. 1. We neglected the contribution by the fainter companion. Weaker red-shifted lines from a fainter companion are present in our spectra. Carney et al. (1994) classified this star as SB2, and Nissen et al. (2004) confirmed it. Latham et al. (2002) computed the period of the orbit (P = 493.00 d).
13. HD 219175: for this star we find different temperature determinations: $T_{\rm eff}$ (adopted) = 5756 K (Gratton et al. 2003); $T_{\rm eff}(B-V)$ = 5844 K; $T_{\rm eff}(H_\alpha)$ = 5856 K

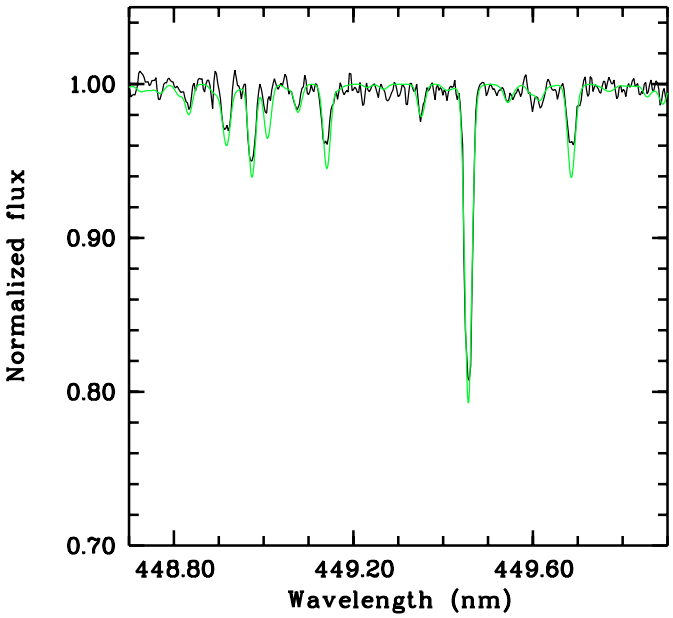

Fig. A.1. G 76 –21 is suspected of being a double-lined system. In fact, lines: Fe II 448.9183 nm, Fe II 449.1405 nm, and Cr I 449.6852 nm show a flat and double core. The grey line is a synthetic spectrum computed with the appropriate parameters.

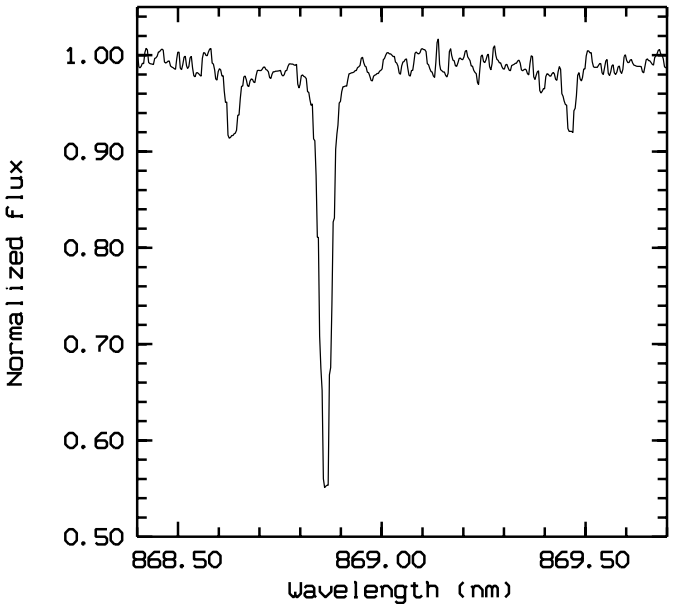

Fig. A.2. HD 219175 shows a flat core of Si I 868.6352 nm, Fe I 868.8624 nm and S I 869.3931 nm and 869.4626 nm.

(Gratton et al. 2003). From the fit of H_α wings, we obtained $T_{\rm eff}(H_\alpha)$ = 6050 K. Moreover, many metal line cores are flat and their profiles are slightly asymmetric. This fact is evident in sulphur lines (see for example Fig. A.2). From these facts we suspect this star of being double.

Table A.1. Observational data.

HD	Rem	BD/CD	G	HIP	α(2000)	δ(2000)	JD–2 400 000.5	*S/N*	Telescope
3567		–09 122	270–23	3026	00 38 32	–08 18 33	50 085.050970000	135	ESONTTB
							52 152.248250600	240	ESO-VLT-U2
		–35 0360	269–87	5004	01 04 06	–34 40 29	51 794.410460600	160	ESO-VLT-U2
			268–32	3446	00 44 04	–13 55 26	52 151.407573600	130	ESO-VLT-U2
		–61 282		7459	01 36 06	–61 05 03	50 085.077490000	130	ESONTTB
							52 149.299538900	250	ESO-VLT-U2
10607		–68 74		7869	01 41 15	–67 40 37	51 795.410954400	190	ESO-VLT-U2
		+02 263	71–33		01 45 14	+03 30.8	52 150.425270600	210	ESO-VLT-U2
16031		–13 482		11952	02 34 11	–12 23 03	52 148.421848000	190	ESO-VLT-U2
17072		–69 109		12485	02 40 40	–69 13 59	52 148.415905600	300	ESO-VLT-U2
		+09 352	76–21	12529	02 41 14	+09 46 12	52 152.387601800	280	ESO-VLT-U2
17288		–60 545		12772	02 44 10	–60 03 22	50 088.054370000	150	ESONTTB
			4-37	12807	02 44 35	+08 28 50	52 151.425852800	130	ESO-VLT-U2
17820		+10 380	4–44	13366	02 51 58	+11 22 12	50 086.047990000	130	ESONTTB
			75–56		03 00 23	–05 57.9	52 150.416166100	130	ESO-VLT-U2
219175 B		–09 6150	157–33	114703	23 14 08	–08 55 53	52 148.209896900	200	ESO-VLT-U2
		+20 571	5–40		03 27 40	+21 02 30	50 087.043650000	130	ESONTTB
							50 087.088760000	150	ESONTTB
		–47 1087		16691	03 34 44	–47 16 12	50 088.172160000	160	ESONTTB
22879		–03 592	80–15	17147	03 40 22	–03 13 01	50 086.065390000	300	ESONTTB
24339		–26 1453		18045	03 51 24	–25 55 57	50 086.075810000	140	ESONTTB
25704		–57 806		18802	04 01 45	–57 12 25	50 085.128840000	200	ESONTTB
							52 148.418458500	240	ESO-VLT-U2
29907	SB	–65 253		21609	04 38 22	–65 24 58	51 793.386280600	130	ESO-VLT-U2
							51 793.392945400	150	ESO-VLT-U2
31128		–27 666		22632	04 52 10	–27 03 51	51 798.410397500	140	ESO-VLT-U2
							51 798.414197000	150	ESO-VLT-U2
241253		+05 824	84–37	24030	05 09 57	+05 33 27	50 087.134130000	150	ESONTTB
34328		–59 1024		24316	05 13 05	–59 38 44	52 150.409787400	270	ESO-VLT-U2
							52 152.403019500	290	ESO-VLT-U2
		+12 853	102–20	26676	05 40 10	+12 10 41	50 088.099770000	110	ESONTTB
							50 088.127500000	110	ESONTTB
		–33 3337		33221	06 54 48	–33 44 49	50 085.189250000	160	ESONTTB
		–57 1633		34285	07 06 29	–57 27 29	50 085.149660000	160	ESONTTB
		–45 3283		36818	07 34 19	–45 16 43	50 086.130080000	100	ESONTTB
							50 086.168240000	100	ESONTTB
							50 087.172990000	100	ESONTTB
60319			88–40	36849	07 34 35	+16 54 04	50 086.206630000	120	ESONTTB
76932		–15 2656		44075	08 58 44	–16 07 58	50 086.223880000	300	ESONTTB
			46–31	45554	09 17 04	+03 11 30	50 085.236710000	70	ESONTTB
							50 085.289440000	70	ESONTTB
103723		–20 3540		58229	11 56 36	–21 25 10	50 087.293330000	180	ESONTTB
105004		–25 9024		58962	12 05 25	–26 35 44	50 088.217500000	130	ESONTTB
							50 088.248700000	130	ESONTTB
106038			12–21	59490	12 12 01	+13 15 41	50 088.311460000	150	ESONTTB
106516		–09 3468		59750	12 15 11	–10 18 45	50 086.372820000	200	ESONTTB
108177	var	+02 2538	13–35	60632	12 25 34	+01 17 02	51 712.953051600	220	ESO-VLT-U2
113679		–37 8363		63918	13 05 53	–38 31 00	50 085.335050000	40	ESONTTB
116064		–38 8457		65201	13 21 44	–39 18 40	51 710.943455200	200	ESO-VLT-U2
120559		–56 5169		67655	13 51 40	–57 26 08	50 088.356550000	190	ESONTTB
							51 712.960426500	120	ESO-VLT-U2

Table A.1. continued.

HD	Rem	BD/CD	G	HIP	α(2000)	δ(2000)	JD–2 400 000.5	*S/N*	Telescope
121004		–45 8786		67863	13 53 58	–46 32 19	50 087.338450000	170	ESONTTB
							51 710.950792700	170	ESO-VLT-U2
							51 710.954920400	180	ESO-VLT-U2
126681		–17 4092		70681	14 27 24	–18 24 40	50 087.355790000	150	ESONTTB
							51 710.960529500	200	ESO-VLT-U2
132475		–21 4009		73385	14 59 49	–22 00 45	51 710.966872900	260	ESO-VLT-U2
							51 710.970791200	300	ESO-VLT-U2
134169		+04 2969		74079	15 08 18	+03 55 50	51 712.964251700	210	ESO-VLT-U2
							51 253.364397300	140	ESO-NTT
							51 253.370955200	240	ESO-NTT
							51 254.334815600	140	ESO-NTT
134439		–15 4042		74235	15 10 13	–16 22 46	51 712.968485700	210	ESO-VLT-U2
134440	var	–15 4041		74234	15 10 13	–16 27 47	51 710.982380800	200	ESO-VLT-U2
140283	var	–10 4149		76976	15 43 03	–10 56 01	50 671.031801400	400	ESO-NTT
							50 672.106291600	400	ESO-NTT
							51 710.977184700	200	ESO-VLT-U2
145417		–57 6303		79537	16 13 49	–57 34 14	51 712.976075800	140	ESO-VLT-U2
159482		+06 3455	139–48	86013	17 34 43	+06 00 52	51 792.972807700	160	ESO-VLT-U2
		+02 3375	20–8	86443	17 39 46	+02 25 00	52 147.975386100	210	ESO-VLT-U2
		+01 3597	20–24	88827	18 07 57	+01 52 33	52 148.971696400	130	ESO-VLT-U2
		+05 3640	140–46	89215	18 12 22	+05 24 04	51 792.984363300	170	ESO-VLT-U2
166913		–59 6824		89554	18 16 26	–59 24 11	51 793.972600100	160	ESO-VLT-U2
							51 795.971286800	160	ESO-VLT-U2
			141–15		18 31 51	+08 35.9	52 149.977870000	60	ESO-VLT-U2
							52 150.963383100	130	ESO-VLT-U2
		+13 3683	141–19	90957	18 33 17	+13 09 25	52 152.009915900	350	ESO-VLT-U2
			21–22		18 39 10	+00 07 14	52 148.961440500	230	ESO-VLT-U2
181743		–45 13178		95333	19 23 42	–45 04 56	51 711.430220700	150	ESO-VLT-U2
							51 793.978402000	180	ESO-VLT-U2
188510		+10 4091	143–17	98020	19 55 10	+10 44 27	51 713.413541900	210	ESO-VLT-U2
							51 794.983357300	140	ESO-VLT-U2
189558		–12 5613		98532	20 01 00	–12 15 20	51 713.417238400	200	ESO-VLT-U2
193901		–21 5703		100568	20 23 36	–21 22 14	51 713.419771300	200	ESO-VLT-U2
194598		+09 4529	144–6	100792	20 26 12	+09 27 00	51 713.423928600	200	ESO-VLT-U2
196892		–19 5889		102046	20 40 49	–18 47 33	52 147.966235700	400	ESO-VLT-U2
		+04 4551		102718	20 48 51	+05 11 59	52 152.141828300	80	ESO-VLT-U2
							52 152.155864400	100	ESO-VLT-U2
204155		+04 4674	25–29	105888	21 26 43	+05 26 30	51 797.988624500	150	ESO-VLT-U2
205650		–28 17381		106749	21 37 26	–27 38 07	51 795.979057900	150	ESO-VLT-U2
			126–52		22 04 13	+19 32.9	52 152.113631600	200	ESO-VLT-U2
		+17 4708	126–62	109558	22 11 31	+18 05 34	52 152.165720900	320	ESO-VLT-U2
		+07 4841	18–39	110140	22 18 37	+08 26 45	52 152.122973300	200	ESO-VLT-U2
211998		HR 8515			22 24 37	–72 15 20	52 149.189346700	140	ESO-VLT-U2
			18–54	111195	22 31 36	+02 09 44	52 152.073008100	100	ESO-VLT-U2
							52 152.078181500	100	ESO-VLT-U2
219175 A		–09 6149	157–32	114702	23 14 07	–08 55 28	52 148.207974500	120	ESO-VLT-U2
			29–71	117522	23 50 01	+08 43 23	52 151.416852000	200	ESO-VLT-U2
GD660	WD				00 54 15	–19 51.6	52 152.258059200	120	ESO-VLT-U2

Table A.1. continued.

HD	Rem	BD/CD	G	HIP	α(2000)	δ(2000)	JD–2 400 000.5	*S/N*	Telescope
W(GCRV) 7547		–39 7674		61200	12 32 29	–40 05 55	50 086.296490000	100	ESONTTB
							50 086.334640000	100	ESONTTB
							50 088.279920000	100	ESONTTB
			75–31	12294	02 38 22	+02 26 44	50 671.414511900	120	ESO-NTT
							50 671.375687400	120	ESO-NTT
83220		–48 4818		47048	09 35 17	–49 07 49	50 086.232880000	110	ESONTTB
113083		–26 4871		63559	13 01 26	–27 22 28	50 085.366190000	50	ESONTTB
		–21 3420			11 55 29.1	–22 23 04	50 087.230070000	130	ESONTTB
							50 087.261300000	100	ESONTTB

Table A.2. Observational data.

Name	π	RV	U	V	W	$T_{\rm eff}$	$\log g$	[Fe/H]	[S/Fe]	Ref[a]	$R_{\rm min}$	$R_{\rm max}$	$Z_{\rm max}$	e	Pop
	mas			km s^{-1}		K	cgs	dex	dex		kpc	kpc	kpc		
−09 122	9.57	−47	−136	−235	−44	6087	4.16	−1.22	+0.33	1	0.141	10.612	7.615	0.974	3
−35 0360	16.28	+45	+110	−176	−26	5048	4.53	−1.15	+0.54	1	0.926	9.488	0.379	0.822	2
−61 0282	11.63	+221	−238	−260	−37	5831	4.53	−1.25	+0.64	1	0.554	16.694	7.748	0.936	3
−68 74	14.01	−5	−4	−143	+121	5757	4.01	−0.99	+0.35	1	2.430	8.511	4.838	0.556	2
02 263	*	−8	*	*	*	5754	4.87	−2.17	+0.91	1	*	*	*	*	3
−13 482	8.67	+24	−29	−99	−37	6194	4.34	−1.61	+0.32	1	3.447	8.761	0.446	0.435	2
−69 109	7.57	+61	+5	−70	−22	5486	2.63	−0.95	+0.34	1	4.675	8.476	0.206	0.289	2
+09 352	5.22	−64	+126	−207	+150	6020	4.20	−2.09	+0.34	1	0.505	10.789	10.353	0.910	3
−60 545	10.38	+11	+99	−116	+61	5744	4.35	−0.82	+0.17	1	2.830	9.518	1.506	0.542	2
+10 380	15.38	+6	−37	−105	−81	5739	4.12	−0.72	+0.31	1	3.350	8.850	1.641	0.451	2
−09 6150	35.69	−33	+68	−46	−1	5337	4.55	−0.63	+0.60	1	5.492	9.316	0.076	0.258	2
+20 571	*	−117	*	*	*	5863	4.24	−0.83	+0.09	1	*	*	*	*	3
−47 1087	9.28	+11	+88	−69	+54	5625	4.82	−0.79	+0.37	1	4.586	9.639	1.276	0.355	2
−03 592	41.07	+120	+110	−86	−45	5827	4.33	−0.83	+0.14	1, 5	3.679	10.043	0.621	0.464	2
−26 1453	*	+90	*	*	*	5900	4.37	−0.63	+0.21	1	*	*	*	*	3
−57 806	19.02	+55	+129	−67	−8	6194	4.34	−0.91	−0.20	1	4.205	10.982	0.046	0.446	2
−65 253	17.00	+81	+379	−161	+17	5351	4.57	−1.52	+0.21	1	1.016	43.436	1.505	0.954	3
−27 666	15.55	+111	+63	−100	−29	5970	4.45	−1.54	+0.40	1	3.339	8.902	0.290	0.454	2
+05 824	10.29	−15	−10	−94	+89	5897	4.33	−1.08	+0.26	1	4.041	8.656	2.479	0.363	2
−59 1024	14.55	+237	+206	−354	+96	5894	4.49	−1.69	+0.33	1	2.872	15.373	4.796	0.685	3
+12 853	14.30	+28	+22	−74	+60	5388	4.62	<−1.17	<+0.26	1	4.783	8.593	1.341	0.285	2
−33 3337	9.11	+71	−12	−51	−130	6079	4.03	<−1.28	<+0.62	1	6.561	8.872	3.505	0.150	2
−57 1633	10.68	+260	+313	−253	−36	6013	4.34	<−0.84	<+0.05	1	0.355	23.990	11.821	0.971	3
−45 3283	15.32	+316	+225	−263	−89	5692	4.82	<−0.85	<+0.49	1	0.639	14.589	1.811	0.916	3
G 88 − 40	12.15	−35	−59	−90	−54	5967	4.26	−0.80	+0.18	1	3.694	9.298	0.790	0.431	2
−15 2656	46.90	+117	+47	−88	+69	5923	4.14	−0.85	+0.12	1, 4, 5, 6	4.068	8.736	1.679	0.365	2
G 46 − 31	3.79	+218	−84	−416	+10	6021	4.44	<−0.75	<+0.21	1	5.743	10.966	0.325	0.313	3
−20 3540	7.63	+167	+77	−206	+49	6029	4.32	−0.79	+0.05	1, 3	0.316	9.062	5.837	0.933	3
−25 9024	2.68	+120	+217	−545	−410	5831	4.36	−0.80	+0.19	1, 3	7.297	250.067	28.969	0.943	3
G 12 − 21	9.16	+100	−13	−271	+24	6013	4.44	<−1.27	<+0.68	1, 3	0.874	8.518	4.271	0.814	3
−09 3468	44.34	−5	+47	+75	+62	6232	4.29	−0.72	+0.33	1, 4, 5	4.790	9.259	1.222	0.318	2
+02 2538	10.95	+155	−108	−227	+48	6133	4.41	<−1.69	<+0.18	1, 3	0.046	10.048	7.827	0.991	3
−37 8363	6.82	+226	+81	−356	+16	5543	3.88	<−0.70	<+0.34	1	3.420	9.158	0.313	0.456	3
−38 8457	15.54	+145	+104	−227	+112	5964	4.32	−1.84	+0.66	1	0.016	10.637	8.530	0.997	3
−56 5169	40.02	+13	+29	−46	−37	5383	4.57	<−0.94	<+0.36	1	5.863	8.584	0.391	0.188	2
−45 8786	16.73	+245	−63	−255	+98	5686	4.40	−0.76	+0.26	1, 3	0.542	9.533	5.953	0.892	3
−17 4092	19.16	−46	+22	−47	−76	5574	4.55	<−1.14	<+0.41	1	6.156	8.506	1.338	0.160	2
−21 4009	10.85	+176	−42	−366	+54	5541	3.79	−1.67	+0.61	1, 2, 4	4.058	8.849	1.211	0.371	3
+04 2969	16.80	+18	−14	−2	+12	5850	3.95	−0.84	+0.28	1	8.000	9.392	0.250	0.080	2
−15 4042	34.14	+310	−34	+191	+566	4996	4.65	<−1.38	<+0.39	1	*	*	*	*	3
−57 6303	72.75	+9	−27	+9	+104	4869	4.62	<−1.39	<+0.83	1	3.696	8.713	0.273	0.404	2
+06 3455	20.90	−136	+164	−63	+81	5713	4.35	−0.84	+0.42	1	4.172	13.500	2.903	0.528	2
+02 3375	8.35	−380	+350	−244	+83	6018	4.20	−2.37	+0.34	1, 3	0.299	33.959	13.597	0.983	3
+05 3640	17.00	−1	−115	−192	+42	5023	4.61	−1.19	+0.75	1	0.545	10.211	1.966	0.899	3
−59 6824	16.09	−47	+51	−46	+69	6070	4.17	−1.54	+0.44	1	6.045	8.959	1.654	0.194	2
+13 3683	3.57	+86	−315	−187	−95	5726	3.78	−2.43	+0.47	1	0.707	29.153	11.845	0.953	3
G 21 − 22	*	+60	*	*	*	6123	4.28	−0.88	−0.14	1	*	*	*	*	3
−45 13178	11.31	+30	+38	−335	−68	5968	4.40	−1.81	+0.84	1, 3	2.898	8.515	1.058	0.492	3
+10 4091	25.32	−193	+153	−114	+63	5503	4.55	<−1.45	<+0.15	1	2.612	11.302	1.815	0.625	2
−12 5613	14.76	−14	−75	−128	+43	5668	3.79	<−1.18	<+0.40	1	2.330	9.316	1.004	0.600	2

Table A.2. contiued.

Name	π	RV	U	V	W	$T_{\rm eff}$	log g	[Fe/H]	[S/Fe]	Ref[a]	$R_{\rm min}$	$R_{\rm max}$	$Z_{\rm max}$	e	Pop
	mas			km s^{-1}		K	cgs	dex	dex		kpc	kpc	kpc		
−21 5703	22.88	−173	+246	+162	+59	5779	4.54	−1.09	+0.35	1, 3, 4, 5	0.302	11.044	5.427	0.947	2
+09 4529	17.94	−248	+77	−277	−31	6023	4.31	−1.17	+0.36	1, 3, 4	1.009	8.904	0.335	0.796	3
−19 5889	15.78	−34	+2	−130	−31	5893	4.12	−1.16	+0.50	1	2.298	8.466	0.287	0.573	2
+04 4551	1.64	−117	+173	+65	+169	5892	4.14	−1.40	+0.46	1	6.048	38.956	16.758	0.731	3
+04 4674	13.02	−84	+34	−125	−45	5772	4.03	−0.73	+0.42	1	2.493	8.534	0.566	0.548	2
−28 17381	18.61	−105	+121	−83	+12	5810	4.50	−1.16	+0.39	1	3.656	10.328	0.280	0.477	2
+17 4708	8.43	−295	+304	−280	+7	6016	4.04	−1.62	+0.40	1, 3	0.925	22.579	0.329	0.921	3
+07 4841	3.97	−232	+269	−316	−110	5980	4.00	−1.59	+0.54	1	1.930	20.209	1.456	0.826	3
HR 8515	*	31	*	*	*	5211	3.36	−1.56	+0.68	1, 4	*	*	*	*	3
G 018 − 54	8.99	−217	−6	−273	+57	5878	3.93	−1.33	−0.03	1	0.915	8.735	4.303	0.810	3
−09 6149	26.52	−30	+88	−52	−12	5756	4.26	−0.63	+0.57	1	5.021	9.785	0.065	0.322	2
GD660	*	−69	*	*	*	5712	4.50	−1.64	+0.40	1	*	*	*	*	3
CGRV 7547	*	−39	*	*	*	6272	4.03	−0.42	+0.04	1	*	*	*	*	3
G075 031	6.67	+57	+199	−154	+60	5884	4.24	−1.25	+0.52	1	1.439	13.202	2.106	0.803	2
−48 4818	10.41	−15	−3	+15	+14	6503	4.11	>−0.43	>−0.18	1	8.400	10.574	0.295	0.115	2
−21 3420	5.43	+6	+42	−152	−158	5946	4.41	<−1.04	<+0.45	1	2.318	8.594	6.285	0.575	2
HD 2665	2.11	−379	−129	−378	−113	4990	2.50	−1.74	+0.29	2, 4	3.885	13.009	4.128	0.540	3
HD 88609	0.63	−36	−38	−233	+48	4570	7.50	−2.85	+0.39	2, 6	0.133	10.199	7.216	0.974	3
HD 111721	3.29	+25	+130	−524	−283	5010	2.31	−1.27	+0.32	2	6.079	68.092	41.917	0.836	3
HD 165195	2.20	−2	−99	−158	−27	4190	1.00	−1.75	+0.52	2, 6	1.377	9.281	0.458	0.742	2
HD 19445	25.85	−139	−156	−123	−68	5810	4.46	−1.90	+0.43	2, 4	2.289	12.240	1.521	0.685	2
HD 84937	12.44	−17	−226	−237	−9	6300	3.97	−2.06	+0.33	2, 6	0.181	15.577	9.837	0.977	3
HD 94028	19.23	+62	+34	−139	+8	5980	4.30	−1.35	+0.08	2	2.008	8.580	0.182	0.621	2
HD 201891	28.26	−45	−91	−116	−59	5880	4.25	−1.03	+0.17	2, 5, 6	2.690	9.832	1.048	0.570	2
HD 201889	17.95	−102	+129	−82	−37	5615	4.24	−0.71	+0.27	2, 4	3.642	10.728	0.477	0.493	2
−13 3442	*	*	*	*	*	6500	4.16	−2.61	+0.30	3	*	*	*	*	3
−30 18140	7.32	+18	−60	−201	−19	6272	4.13	−1.88	+0.25	3	0.364	8.829	5.607	0.921	3
−35 14849	6.45	+103	−147	−325	−54	6125	4.11	−2.41	+0.31	3	2.151	11.557	0.987	0.686	3
−42 14278	5.84	+152	−203	−320	+117	5812	4.25	−2.12	+0.30	3	2.065	16.602	6.929	0.779	3
HD 110621	7.06	+219	+15	−259	+53	5989	3.99	−1.66	+0.32	3	0.591	8.614	4.159	0.871	3
HD 140283	17.44	−171	+250	−253	+42	5690	3.69	−2.42	+0.31	3	0.384	16.200	9.986	0.954	3
HD 146296	*	*	*	*	*	5671	4.17	−0.74	+0.20	3	*	*	*	*	3
HD 148816	24.34	−52	−83	−264	−81	5823	4.14	−0.73	+0.24	3, 5	0.695	9.707	5.111	0.866	3
HD 160617	8.66	+100	−55	−215	−94	5931	3.77	−1.79	+0.39	3	0.139	9.298	6.528	0.971	3
HD 179626	7.52	−71	−142	−318	+52	5699	3.92	−1.14	+0.29	3	2.001	11.231	1.415	0.698	3
HD 188031	4.78	−139	+186	−414	−9	6054	4.03	−1.79	+0.32	3	4.467	15.120	0.148	0.544	3
HD 215801	4.84	−86	+17	−285	+129	6005	3.81	−2.29	+0.28	3	1.751	8.401	5.838	0.655	3
LP 815 − 43	*	*	*	*	*	6533	4.25	−2.67	+0.24	3	*	*	*	*	3
G 011 − 044	4.76	+98	−169	−398	−118	5995	4.29	−2.09	+0.38	3	4.357	16.674	4.779	0.586	3
G 013 − 009	5.75	+56	+104	−267	−95	6360	4.01	−2.27	+0.46	3	0.717	10.039	1.745	0.867	3
G 016 − 013	3.62	−52	+40	−364	+82	5602	4.17	−0.76	+0.29	3	4.202	8.485	2.160	0.338	3
G 018 − 039	3.97	−235	+269	−318	−107	5910	4.09	−1.52	+0.37	3	*	*	*	*	3
G 024 − 003	5.31	−209	+1	−274	+80	5910	4.16	−1.67	+0.38	3	0.919	8.822	4.480	0.811	3
G 029 − 023	*	*	*	*	*	5966	3.82	−1.80	+0.30	3	*	*	*	*	3
G 053 − 041	1.72	+88	+63	−782	−559	5829	4.15	−1.34	+0.29	3	8.684	1785.388	0.425	0.990	3
G 064 − 012	1.88	+443	+161	−623	+401	6511	4.39	−3.17	+0.36	3	8.278	480.982	456.608	0.966	3
G 064 − 037	2.88	+91	−270	−557	−257	6318	4.16	−3.12	+0.34	3	5.543	174.859	60.746	0.939	3
G 066 − 030	*	*	*	*	*	6346	4.24	−1.52	+0.24	3	*	*	*	*	3
G 186 − 026	7.49	−319	+48	−344	−93	6273	4.25	−2.62	+0.19	3	3.366	8.635	2.033	0.439	3
HD 2796	*	*	*	*	*	4867	1.80	−2.30	+0.81	4	*	*	*	*	3

Table A.2. contiued.

Name	π	RV	U	V	W	$T_{\rm eff}$	log g	[Fe/H]	[S/Fe]	Ref[a]	$R_{\rm min}$	$R_{\rm max}$	$Z_{\rm max}$	e	Pop
	mas			km s^{-1}		K	cgs	dex	dex		kpc	kpc	kpc		
HD 157214	*	*	*	*	*	5625	4.36	−0.32	+0.19	4	*	*	*	*	3
HD 1461	42.67	−11	+32	−39	−1	6193	4.11	+0.47	−0.20	5	6.211	8.650	0.073	0.164	1
HD 9826	74.25	−28	−29	−22	−14	6119	4.12	+0.12	−0.14	5, 7	6.901	9.186	0.084	0.142	1
HD 10453	26.83	−10	−36	−64	−9	6368	3.96	−0.46	+0.17	5	4.797	8.902	0.043	0.300	2
HD 13540	17.75	+14	+2	+17	−3	6301	4.12	−0.43	+0.19	5	8.518	10.686	0.055	0.113	1
HD 16895	*	*	*	*	*	6228	4.27	+0.01	+0.01	5	*	*	*	*	4
HD 17948	37.78	+29	+31	+9	+13	6455	4.20	−0.26	−0.00	5, 6	8.297	10.170	0.271	0.101	1
HD 28620	23.09	+21	+22	+0	+0	6114	4.11	−0.38	+0.06	5	8.393	9.286	0.090	0.051	1
HD 30652	24.60	+24	+41	−57	+60	6424	4.28	+0.04	−0.02	5	7.710	8.735	0.134	0.062	1
HD 33564	47.66	−10	−19	+6	−3	6276	4.16	+0.05	+0.05	5	8.095	10.088	0.045	0.110	1
HD 39315	14.93	−22	−25	+27	−1	6202	3.83	−0.38	+0.16	5	8.283	12.259	0.087	0.194	2
HD 49933	33.45	−15	−26	−13	−9	6592	4.21	−0.42	+0.06	5, 6	7.370	9.401	0.024	0.121	1
HD 58461	28.72	+7	+17	+4	−29	6562	4.11	−0.15	−0.05	5	8.488	9.518	0.293	0.057	1
HD 77967	24.57	−43	−63	−1	+5	6329	4.15	−0.46	+0.11	5	7.023	11.368	0.172	0.236	2
HD 82328	74.15	+15	+57	−34	−24	6308	3.84	−0.13	−0.09	5	6.185	9.218	0.214	0.197	2
HD 84737	54.26	+5	−12	−6	+17	5813	4.12	+0.13	−0.10	5	8.007	9.230	0.325	0.071	4
HD 94388	31.91	−5	−29	−10	−22	6379	3.96	+0.07	+0.05	5	7.395	9.577	0.188	0.129	1
HD 150177	23.02	−18	+6	−24	−25	6061	3.93	−0.63	+0.17	5	7.206	8.471	0.213	0.081	1
HD 159307	13.40	−20	+13	−23	+3	6237	3.93	−0.65	+0.24	5	7.225	8.443	0.114	0.078	1
HD 162003	45.38	−10	−30	−3	−5	6498	4.02	+0.02	−0.08	5	7.657	9.909	0.036	0.128	1
HD 168151	42.56	−35	+6	−13	−51	6530	4.12	−0.28	+0.09	5	8.166	8.530	0.658	0.022	2
HD 187013	47.94	+5	−37	−7	−24	6298	4.15	−0.02	−0.09	5	7.343	9.953	0.213	0.151	2
HD 215648	61.54	−5	−4	−32	−28	6158	3.96	−0.24	+0.05	5	6.728	8.574	0.254	0.121	2
HD 216106	15.03	−44	−37	−41	−32	5923	3.74	−0.16	+0.04	5	5.939	9.112	0.331	0.211	2
HD 222368	72.51	+5	+8	−27	−26	6178	4.08	−0.13	+0.06	5	7.094	8.502	0.227	0.090	1
HD 59984	33.40	+55	+29	−51	−18	5896	3.93	−0.88	+0.20	5, 6	5.622	8.606	0.127	0.210	2
HD 63077	65.79	+103	+146	−58	+40	5825	4.15	−0.89	+0.32	5	4.366	12.113	0.949	0.470	2
HD 69897	55.17	+32	+24	−38	+7	6227	4.20	−0.50	+0.16	5, 6	6.316	8.578	0.168	0.152	1
HD 88218	32.55	+41	+53	−49	−24	5661	3.94	−0.53	+0.27	5	5.530	8.935	0.206	0.235	2
HD 91324	45.72	+20	+43	−30	−2	6123	3.95	−0.60	+0.11	5	6.585	8.890	0.056	0.149	1
HD 102365	8.23	+15	+852	−327	−3	5562	4.39	−0.39	+0.04	5	6.013	9.233	0.143	0.211	3
HD 136352	68.70	−69	+119	−47	+36	5584	4.27	−0.58	+0.14	5	4.987	11.142	0.802	0.382	2
HD 139211	32.34	−22	+38	−13	−13	6231	4.12	−0.26	+0.10	5	7.528	9.071	0.069	0.093	1
HD 157089	25.88	−162	+167	−42	−10	5712	4.00	−0.79	+0.35	5	4.576	13.775	0.052	0.501	2
HD 203608	8.50	−30	−62	+419	−152	6094	4.29	−0.91	+0.22	5	8.492	13.606	0.203	0.231	2
HD 44007	5.17	+167	+84	−167	+11	4910	2.47	−1.49	+0.29	6	1.227	9.178	0.483	0.764	2
HD 175305	6.18	−181	+74	−81	−291	5170	2.64	−1.21	+0.04	6	4.218	22.975	19.991	0.690	3
HD 184266	3.28	−348	+313	−330	−176	5640	2.17	−1.53	+0.43	6	2.095	35.448	18.863	0.888	3
HD 3795	35.02	−53	+47	−91	+47	5330	3.80	−0.85	+0.39	6	3.810	8.743	0.910	0.393	2
HD 6582	32.40	−97	+348	−399	−186	5340	4.42	−0.84	+0.38	6	*	*	*	*	3
HD 13555	33.19	+6	+20	−12	+4	6470	3.90	−0.27	+0.02	6	7.973	8.678	0.130	0.042	1
HD 14412	78.88	+7	+11	+27	−10	5340	4.44	−0.47	+0.10	6	8.503	11.574	0.035	0.153	1
HD 15335	32.48	+40	+25	+32	−14	5840	3.89	−0.37	+0.24	6	8.470	12.251	0.099	0.182	2
HD 18768	21.65	+97	+88	+38	−21	5750	3.84	−0.70	+0.34	6	7.679	15.209	0.235	0.329	3
HD 22484	72.89	+28	−1	−15	−42	5960	4.02	−0.25	+0.17	6	7.836	8.661	0.482	0.050	2
HD 33256	39.99	+9	+9	−6	+2	6440	3.99	−0.37	+0.07	6	8.509	8.597	0.110	0.005	1
HD 37495	23.54	+36	+26	−17	−21	6350	3.74	−0.31	+0.38	6	7.583	8.716	0.163	0.069	1
HD 40136	66.47	−2	+5	+9	+2	7190	4.15	−0.02	+0.03	6	8.495	9.854	0.113	0.074	1
HD 60532	38.91	+61	+39	−48	−3	6150	3.69	−0.35	+0.20	6	5.720	8.721	0.050	0.208	2
HD 62301	29.22	−3	+8	−109	−22	5900	4.09	−0.71	+0.25	6	3.048	8.627	0.179	0.478	2

Table A.2. contiued.

Name	π	RV	U	V	W	$T_{\rm eff}$	$\log g$	[Fe/H]	[S/Fe]	Ref[a]	$R_{\rm min}$	$R_{\rm max}$	$Z_{\rm max}$	e	Pop
	mas			km s^{-1}		K	cgs	dex	dex		kpc	kpc	kpc		
HD 142860	89.92	+7	−56	−33	−24	6240	4.09	−0.32	+0.17	6	5.969	9.787	0.220	0.242	2
HD 165908	63.88	+1	+6	+1	+9	5900	4.09	−0.64	+0.15	6	8.474	9.114	0.204	0.036	1
HD 182572	66.01	−100	+116	−30	−20	5500	4.07	+0.23	+0.23	6	5.526	11.481	0.185	0.350	4
HD 207978	36.15	+19	−14	+16	−7	6400	4.03	−0.63	+0.10	6	8.308	10.725	0.011	0.127	1
HD 216385	37.25	+12	+58	−7	−34	6300	3.91	−0.27	+0.09	6	7.334	10.080	0.383	0.158	2
HD 217107	50.71	−14	+2	−9	+11	5490	4.15	+0.22	+0.20	6	8.192	8.662	0.218	0.028	1
HD 218470	29.33	−2	+30	−9	+10	6600	4.01	−0.15	−0.02	6	7.895	9.034	0.213	0.067	1
HD 142	39.00	+3	+58	−37	−13	6302	4.34	+0.14	−0.39	7	6.047	9.180	0.069	0.206	4
HD 1237	56.76	−6	+33	−16	+2	5536	4.56	+0.12	−0.22	7	7.466	8.870	0.112	0.086	1
HD 2039	11.13	+8	+29	−15	−14	5976	4.45	+0.32	−0.17	7	7.638	8.755	0.111	0.068	1
HD 3651	90.03	−34	−41	−20	+9	5173	4.37	+0.12	+0.11	7	6.781	9.611	0.209	0.173	4
HD 4203	*	*	*	*	*	5636	4.23	+0.40	−0.20	7	*	*	*	*	4
HD 4208	30.58	+55	+53	−5	−56	5626	4.49	−0.24	−0.14	7	7.585	10.122	0.879	0.143	2
HD 6434	24.80	+22	−85	−67	−2	5835	4.60	−0.52	−0.18	7	4.328	10.082	0.075	0.399	2
HD 8574	22.65	+19	+44	−37	−31	6151	4.51	+0.06	−0.11	7	6.247	8.910	0.304	0.176	4
HD 10647	57.63	+13	+3	−20	−5	6143	4.48	−0.03	−0.12	7	7.483	8.533	0.030	0.066	1
HD 10697	30.71	−44	−35	−27	+15	5641	4.05	+0.14	−0.19	7	6.604	9.305	0.296	0.170	4
HD 12661	*	*	*	*	*	5702	4.33	+0.36	−0.26	7	*	*	*	*	4
HD 13445	91.63	+53	+98	−74	−26	5163	4.52	−0.24	−0.01	7	4.154	9.777	0.257	0.404	2
HD 16141	27.85	−53	−86	−41	+3	5801	4.22	+0.15	−0.12	7	5.283	10.661	0.139	0.337	4
HD 17051	58.00	+16	+31	−17	−8	6252	4.61	+0.26	−0.26	7	7.497	8.828	0.016	0.082	1
HD 19994	44.69	+18	+20	−20	−6	6190	4.19	+0.24	−0.29	7	7.505	8.586	0.020	0.067	1
HD 22049	10.75	+16	−190	+289	−257	5073	4.43	−0.13	+0.00	7	8.469	9.708	0.159	0.068	1
HD 23079	28.90	+0	−28	+15	−16	5959	4.35	−0.11	−0.24	7	8.037	11.079	0.115	0.159	1
HD 23596	19.24	−10	−4	−10	+14	6108	4.25	+0.31	−0.23	7	8.083	8.854	0.267	0.046	1
HD 28185	25.28	+50	+33	−35	−23	5656	4.45	+0.22	−0.09	7	6.489	8.715	0.190	0.146	1
HD 30177	*	*	*	*	*	5587	4.29	+0.38	−0.23	7	*	*	*	*	4
HD 33636	34.85	+5	+0	−30	+9	6046	4.71	−0.08	−0.12	7	6.856	8.570	0.193	0.111	1
HD 37124	30.08	−12	−22	−47	−44	5546	4.50	−0.38	+0.16	7	5.788	8.801	0.545	0.207	2
HD 38529	23.57	+29	+12	−25	−34	5674	3.94	+0.40	−0.33	7	7.278	8.540	0.344	0.080	4
HD 39091	54.92	+9	+83	−47	+2	5991	4.42	+0.10	−0.18	7	5.362	9.731	0.083	0.289	4
HD 40979	30.00	+33	+37	−21	+8	6145	4.31	+0.21	−0.21	7	7.169	8.930	0.189	0.109	1
HD 46375	29.93	+1	−9	−20	+9	5268	4.41	+0.20	+0.03	7	7.361	8.757	0.194	0.087	1
HD 47536	+8.24	+79	+55	−79	+46	4554	2.48	−0.54	+0.26	7	4.327	8.915	0.930	0.346	2
HD 49674	24.55	+12	+14	−24	+1	5644	4.37	+0.33	−0.20	7	7.302	8.548	0.098	0.079	1
HD 50554	32.23	−4	−4	−10	−12	6026	4.41	+0.01	−0.34	7	8.005	8.820	0.050	0.048	1
HD 52265	35.63	+53	+52	−20	−9	6105	4.28	+0.23	−0.21	7	6.946	9.338	0.024	0.147	1
HD 65216	28.10	+42	+27	−41	−20	5666	4.53	−0.12	−0.03	7	6.139	8.574	0.152	0.166	2
HD 68988	17.00	−70	−75	−22	−10	5988	4.45	+0.36	−0.19	7	6.176	10.912	0.050	0.277	4
HD 72659	19.47	−18	−7	−2	−40	5995	4.30	+0.03	−0.26	7	8.214	9.387	0.478	0.067	4
HD 73256	27.38	+30	+36	−21	−15	5518	4.42	+0.26	−0.24	7	7.194	8.876	0.089	0.105	1
HD 73526	10.57	+26	+77	−14	+23	5699	4.27	+0.27	−0.22	7	6.815	10.465	0.444	0.211	4
HD 74156	15.49	+4	−29	−52	−18	6112	4.34	+0.16	−0.29	7	5.438	8.903	0.133	0.242	4
HD 75289	34.55	+14	−20	−17	−22	6143	4.42	+0.28	−0.31	7	7.268	9.089	0.174	0.111	1
HD 75732	79.80	+27	+37	−18	−8	5279	4.37	+0.33	−0.21	7	7.322	8.950	0.017	0.100	1
HD 76700	16.75	+37	+69	−42	−49	5737	4.25	+0.41	−0.31	7	5.829	9.422	0.688	0.236	4
HD 80606	17.13	+3	−7	+3	+11	5574	4.46	+0.32	−0.22	7	8.330	9.605	0.242	0.071	1
HD 82943	36.42	+8	−10	−20	−9	6015	4.46	+0.30	−0.20	7	7.317	8.779	0.023	0.091	1
HD 83443	22.97	+28	−20	−29	−12	5454	4.33	+0.35	−0.15	7	6.639	8.875	0.056	0.144	1

Table A.2. contiued.

Name	π	RV	U	V	W	$T_{\rm eff}$	$\log g$	[Fe/H]	[S/Fe]	Ref[a]	$R_{\rm min}$	$R_{\rm max}$	$Z_{\rm max}$	e	Pop
	mas			km s^{-1}		K	cgs	dex	dex		kpc	kpc	kpc		
HD 92788	30.94	−5	−16	−22	−21	5821	4.45	+0.32	−0.22	7	7.114	8.889	0.168	0.111	1
HD 95128	71.04	+13	+25	−2	+2	5954	4.44	+0.06	−0.16	7	8.244	9.139	0.107	0.051	1
HD 106252	26.71	+15	−29	−44	+0	5899	4.34	−0.01	−0.09	7	5.823	8.901	0.098	0.209	2
HD 108147	25.93	−5	+30	−11	−14	6248	4.49	+0.20	−0.25	7	7.777	8.886	0.081	0.067	1
HD 111232	34.63	+102	−59	−85	+5	5494	4.50	−0.36	+0.08	7	3.812	9.201	0.155	0.414	2
HD 114762	24.65	+50	+83	−70	+58	5884	4.22	−0.70	+0.15	7	4.581	9.517	1.358	0.350	2
HD 114783	48.95	−13	+16	−2	−10	5098	4.45	+0.09	+0.01	7	8.434	8.884	0.032	0.026	1
HD 117176	55.22	+5	−13	−52	−4	5560	4.07	−0.06	+0.04	7	5.513	8.621	0.041	0.220	2
HD 120136	64.12	−16	+33	−19	−7	6339	4.19	+0.23	−0.18	7	5.923	15.917	0.022	0.458	4
HD 121504	22.54	+19	+28	−52	−2	6075	4.64	+0.16	−0.16	7	5.537	8.542	0.061	0.213	4
HD 130322	33.60	−12	+9	−26	−11	5392	4.48	+0.03	−0.06	7	7.093	8.482	0.048	0.089	1
HD 134987	38.98	+3	+22	−40	+20	5776	4.36	+0.30	−0.18	7	6.276	8.525	0.354	0.152	4
HD 136118	19.13	−4	+21	−16	+17	6222	4.27	−0.04	−0.21	7	6.529	11.193	0.389	0.263	2
HD 141937	29.89	−3	−3	+13	−9	5909	4.51	+0.10	−0.18	7	8.398	10.267	0.026	0.100	1
HD 142415	28.93	−12	+24	−13	+0	6045	4.53	+0.21	−0.09	7	7.787	8.682	0.087	0.054	1
HD 143761	57.38	+18	−55	−36	+21	5853	4.41	−0.21	−0.04	7	5.928	9.681	0.382	0.240	2
HD 145675	55.11	−6	−26	−7	−10	5311	4.42	+0.43	−0.13	7	7.591	9.564	0.036	0.115	1
HD 147513	77.69	+10	−11	+0	−2	5883	4.51	+0.06	−0.21	7	8.127	9.429	0.065	0.074	1
HD 160691	65.46	−9	+14	−8	−4	5798	4.31	+0.32	−0.17	7	8.294	8.535	0.036	0.014	1
HD 168443	26.40	−49	+30	−58	−7	5617	4.22	+0.06	−0.04	7	5.208	8.552	0.008	0.243	4
HD 168746	23.19	−26	+19	−22	−3	5601	4.41	−0.08	+0.13	7	7.285	8.518	0.046	0.078	1
HD 169830	27.53	−17	+17	+1	+4	6299	4.10	+0.21	−0.31	7	8.407	9.161	0.131	0.043	1
HD 178911	20.42	−41	+59	−20	+1	5600	4.44	+0.27	−0.10	7	6.763	9.559	0.095	0.171	4
HD 179949	36.97	−26	+27	−13	−11	6260	4.43	+0.22	−0.15	7	7.730	8.781	0.044	0.064	1
HD 186427	46.70	−27	−18	−30	−2	5772	4.40	+0.08	−0.13	7	6.676	8.793	0.065	0.137	1
HD 187123	20.87	−18	−2	−16	−43	5845	4.42	+0.13	−0.23	7	7.780	8.627	0.512	0.052	4
HD 190228	16.10	−49	+19	−46	−36	5325	3.90	−0.26	+0.01	7	5.929	8.505	0.375	0.178	2
HD 190360	62.92	−45	+12	−45	−64	5584	4.37	+0.24	−0.14	7	6.194	8.496	0.993	0.157	4
HD 192263	50.27	−11	+16	+11	+20	4947	4.51	−0.02	−0.08	7	8.458	10.055	0.382	0.086	2
HD 195019	26.77	−93	+73	−77	−37	5859	4.32	+0.09	−0.24	7	4.185	9.133	0.425	0.371	4
HD 202206	*	*	*	*	*	5752	4.50	+0.35	−0.23	7	*	*	*	*	4
HD 209458	21.24	−15	+6	−16	+1	6117	4.48	+0.02	−0.22	7	7.805	8.503	0.091	0.043	1
HD 210277	46.97	−24	−3	−52	−4	5532	4.29	+0.19	−0.07	7	5.551	8.528	0.041	0.211	4
HD 213240	24.54	−0	−25	−30	+23	5984	4.25	+0.17	−0.27	7	6.584	8.965	0.423	0.153	4
HD 216435	30.04	−1	+28	−22	−10	5938	4.12	+0.24	−0.14	7	7.245	8.662	0.046	0.089	1
HD 216437	37.71	−3	−3	+11	−1	5887	4.30	+0.25	−0.15	7	8.393	10.059	0.080	0.090	1
HD 216770	26.39	+31	+12	−36	−47	5423	4.40	+0.26	−0.01	7	6.600	8.488	0.589	0.125	4
HD 217014	65.10	−31	+15	−28	+15	5804	4.42	+0.20	−0.13	7	7.004	8.515	0.267	0.097	1
HD 222404	72.50	−42	−22	−37	−3	4916	3.36	+0.16	−0.11	7	6.217	8.815	0.052	0.173	1
HD 222582	23.84	+12	−37	−1	−11	5843	4.45	+0.05	−0.25	7	7.555	10.259	0.061	0.152	1
HD 1581	16.38	+9	+534	+0	−270	5956	4.39	−0.14	−0.28	7	7.179	10.845	0.613	0.203	2
HD 4391	66.92	11	+16	+1	+8	5878	4.74	−0.03	−0.02	7	8.454	9.155	0.192	0.040	1
HD 5133	71.01	−7	+36	−21	+7	4911	4.49	−0.17	−0.23	7	7.202	8.886	0.172	0.105	1
HD 7570	66.43	+12	+44	−22	−10	6140	4.39	+0.18	−0.18	7	7.000	9.080	0.040	0.129	1
HD 10360	*	*	*	*	*	4970	4.49	−0.26	+0.06	7	*	*	*	*	3
HD 10700	74.17	−16	−56	+110	+4	5344	4.57	−0.52	+0.07	7	8.314	12.255	0.301	0.192	2
HD 17925	96.33	+19	+16	−22	−10	5180	4.44	+0.06	−0.14	7	7.364	8.526	0.030	0.073	1
HD 20010	70.86	−20	+37	+17	+32	6275	4.40	−0.19	+0.02	7	8.274	11.213	0.683	0.151	2
HD 20766	82.51	+12	+70	−47	+16	5733	4.55	−0.21	−0.09	7	5.473	9.374	0.310	0.263	2
HD 20794	65.02	+87	+174	−166	+39	5444	4.47	−0.38	+0.03	7	*	*	*	*	3

Table A.2. contiued.

Name	π	RV	U	V	W	$T_{\rm eff}$	log g	[Fe/H]	[S/Fe]	Ref[a]	$R_{\rm min}$	$R_{\rm max}$	$Z_{\rm max}$	e	Pop
	mas			km s^{-1}		K	cgs	dex	dex		kpc	kpc	kpc		
HD 20807	82.79	+12	+70	−47	+17	5843	4.47	−0.23	−0.07	7	5.516	9.373	0.317	0.259	2
HD 23249	10.58	−6	+179	+267	+93	5074	3.77	+0.13	−0.18	7	8.501	11.638	0.293	0.156	4
HD 23484	61.63	+32	+35	−16	−16	5176	4.41	+0.06	−0.16	7	7.455	8.952	0.109	0.091	1
HD 30495	75.10	+17	+21	−6	+0	5868	4.55	+0.02	−0.12	7	8.243	8.823	0.082	0.034	1
HD 36435	51.10	+13	−9	−3	−18	5479	4.61	+0.00	−0.05	7	8.084	9.226	0.132	0.066	1
HD 38858	64.25	+29	+15	−28	−12	5752	4.53	−0.23	−0.02	7	6.958	8.525	0.048	0.101	1
HD 43162	59.90	+22	+21	−10	−7	5633	4.48	−0.01	−0.17	7	8.071	8.690	0.005	0.037	1
HD 43834	98.54	+35	−19	−29	−12	5594	4.41	+0.10	−0.05	7	6.654	8.828	0.048	0.140	1
HD 53705	61.54	+86	+53	−73	−20	5825	4.37	−0.19	−0.01	7	4.465	8.813	0.156	0.327	2
HD 53706	66.29	+90	+52	−77	−21	5260	4.35	−0.26	+0.16	7	4.291	8.791	0.171	0.344	2
HD 65907	61.76	+14	−12	−24	+34	5979	4.59	−0.29	+0.04	7	7.200	8.785	0.627	0.099	2
HD 69830	79.48	+30	−29	−61	−10	5410	4.38	−0.03	−0.12	7	4.969	8.804	0.032	0.278	2
HD 74576	89.78	+14	+26	−10	−1	5000	4.55	−0.03	−0.07	7	7.953	8.850	0.073	0.053	1
HD 76151	58.50	+28	+38	−17	−13	5803	4.50	+0.14	−0.04	7	7.347	9.007	0.067	0.101	1
HD 84117	67.19	+34	+40	−25	+6	6167	4.35	−0.03	−0.07	7	6.891	8.905	0.160	0.128	1
HD 189567	56.45	−12	+71	−30	−49	5765	4.52	−0.23	−0.07	7	6.221	9.738	0.674	0.220	2
HD 192310	13.33	−54	+274	−1	−356	5069	4.38	−0.01	−0.29	7	6.877	10.341	0.145	0.201	2
HD 196761	68.28	−45	+62	+20	+6	5435	4.48	−0.29	−0.01	7	7.846	12.003	0.185	0.209	2
HD 207129	63.95	−7	+14	−22	+1	5910	4.42	+0.00	−0.05	7	7.350	8.498	0.090	0.072	1
HD 211415	73.47	−14	+30	−41	+7	5890	4.51	−0.17	−0.03	7	6.103	8.612	0.169	0.171	2

The column ("Ref") indicates the source of examined data:
1: this paper; 2: Ryde & Lambert (2004); 3: Nissen et al. (2004); 4: Israelian & Rebolo (2001); 5: Chen et al. (2002); 6: Takada-Hidai et al. (2002) and 7: Ecuvillon et al. (2004).
The last column ("Pop") indicates the kinematic classification of the star:
1 is a thin disk star; 2 is a dissipative component star; 3 is an accretion component; 4 is a star which does not fall in any of the other categories.This classification has been taken from Gratton et al. (2003).